Journal of Power Sources 242 (2013) 486–502

Contents lists available at SciVerse ScienceDirect

Journal of Power Sources

journal homepage: www.elsevier.com/locate/jpowsour

Review

Aluminosilicate-based sealants for SOFCs and other electrochemical applications – A brief review

Dilshat U. Tulyaganov, Allu Amarnath Reddy, Vladislav V. Kharton, José M.F. Ferreira*

Department of Materials and Ceramics Engineering, University of Aveiro, CICECO, 3810-193 Aveiro, Portugal

HIGHLIGHTS

- The state of the art in development of aluminosilicate-based sealants is presented.
- Compatibility of alkali oxides with SOFC components is still unproven.
- Barium-containing boron-aluminosilicate glass sealants offer suitable CTE, T_g and T_s.
- SrO containing clinopyroxene glasses demonstrated suitable sealing properties.

GRAPHICAL ABSTRACT

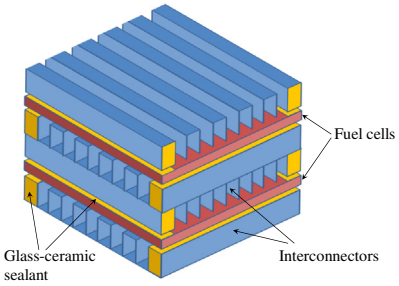

ARTICLE INFO

Article history:
Received 13 March 2013
Received in revised form
10 May 2013
Accepted 27 May 2013
Available online 20 June 2013

Keywords:
Solid oxide fuel cells
Sealants
Glass-ceramics
Coefficient of thermal expansion
Electrical resistivity
Stability

ABSTRACT

Among different designs of solid oxide fuel cells (SOFCs), planar design is the most promising due to easier fabrication, improved performance and relatively high power density. In planar SOFCs and other solid-electrolyte devices, gas-tight seals must be formed along the edges of each cell and between the stack and gas manifolds. For a sealant to work effectively in high-temperature SOFC environment, equilibrium needs to be achieved amid its mechanical properties and flow behavior so that it does not only maintain its hermeticity at high temperature but is also able to reduce mechanical stresses generated in the seal during thermal cycling. The most common sealants based on glass or glass-ceramic materials have been shown to operate in fuel cells for more than 1000 h with no significant degradation.

Analysis of the current literature sources demonstrated that from thermal and chemical stability points of view, silicate based glass systems are more suitable than borate and borosilicate glass systems. In this work, different glass-ceramic (GC) compositions based on alkaline- and alkaline-earth aluminosilicate-based glass systems are reviewed with a special emphasis on their thermal, chemical, mechanical, and electrical properties. Based on these considerations, glass composition design approaches are provided that aid in search of the best seal glasses satisfying the rigid functional requirements. Among all the glass systems studied, a pyroxene based CaO–MgO–SrO–BaO–La_2O_3–Al_2O_3–SiO_2 seal GC compositions have been specifically discussed because those have achieved appropriate thermal and chemical properties along with high stability. Approaches for further developments and optimization of GC sealants are briefly discussed.

1. Introduction

Technologies based on the use of solid oxide electrolytes provide important advantages with respect to the conventional industrial processes. In particular, solid oxide fuel cells (SOFCs) are considered as alternative electric power generation systems due to high

* Corresponding author. Tel.: +351 234 370242; fax: +351 234 370204.
E-mail address: jmf@ua.pt (J.M.F. Ferreira).

0378-7753/$ – see front matter © 2013 Elsevier B.V. All rights reserved.
http://dx.doi.org/10.1016/j.jpowsour.2013.05.099

energy-conversion efficiency, fuel flexibility, environmental safety, low noise, and a possibility to recover exhaust heat [1–3]. A single SOFC comprises, at least, one dense solid-electrolyte (SE) membrane in contact with porous cathode and anode, onto which a gaseous oxidant (usually atmospheric oxygen) and a fuel are continuously supplied; the power is generated due to oxidant reduction at the cathode and fuel oxidation by the O^{2-} anions diffused through the electrolyte, at the anode. The SOFC performance is primarily governed by electrical and electrochemical properties of the electrodes and solid electrolyte, compositions of the fuel and oxidant gas mixtures, current collection, and an absence of gas diffusion limitations [1–7]. Of critical importance for the SOFC efficiency and durability are also the properties of sealants used to prevent gas mixing between the anode and cathode compartments, to bond the cell stacks, and to provide electrical insulation. Similar SE membranes, electrodes and sealants are used for high-temperature electrolyzers of steam and carbon dioxide, oxygen pumps and various amperometric sensors, where the operation principles are based on the oxygen anion transport through the solid electrolyte under applied voltage [4–8]. These devices make it possible to produce high-purity gases such as H_2, CO and O_2, to precisely dose gaseous components, and to measure concentrations and flow rates of oxygen-containing gases. As a rule, the performance of such appliances is even more dependent on the quality and stability of sealing's compared to SOFCs. Whilst the negative impact of minor leakages in the SOFC stacks can often be neglected, any leak may critically increase the contamination of high-purity gases produced using the solid-electrolyte membranes and measuring errors of the electrochemical sensors.

The aim of this review is to analyze available data on the newly reported sealants for SOFCs and other electrochemical devices, based on aluminosilicate glass-ceramics (GCs). Particular attention is focused on their functional properties determining applicability under the SOFC operating conditions, advantages and drawbacks with respect to other known systems, and the effects of various additives enabling sealant optimization. In light of the technological criteria discussed below, the aluminosilicate-based materials constitute one of most promising families of the rigid GC sealants providing, in turn, serious advantages with respect to compressive (e.g. mica-based hybrids) and compliant (e.g. metal-brazes) seals [9–12]. In fact, the latter types of sealing may rarely be used for high-purity gas generators and analytical appliances with solid oxide electrolyte membranes; their application for SOFCs is also associated with significant limitations. Readers interested in other families of the sealants, sealing technologies and stack hermetization methods are referred to relevant reviews and monographs (see [3,4,9,11–13] and references therein). Selection of the references for this review is focused on the last 10–15 years, with the main emphasis on the newly reported materials.

2. Key requirements to seals in SOFCs and other devices

Figs. 1 and 2 present several typical examples illustrating the use of high-temperature sealants in various SOFCs [14–19]. The seal optimization requires always a multifactor analysis; in addition to the materials science-related aspects and sealing configuration, the variables include, at least, contact area with other components of the electrochemical device, compression, exposure to oxidizing and reducing atmospheres, seal formation conditions, and prospective startup/shutdown regimes. Nonetheless, the general requirements to the glass-ceramic sealants, irrespective of the stack configuration and fabrication technologies, involve [2–4,13,20–23]:

(i) Nearly zero gas permeability.
(ii) Good adhesion to the solid electrolyte interconnects, electrodes, current collectors and/or other interfacing materials.

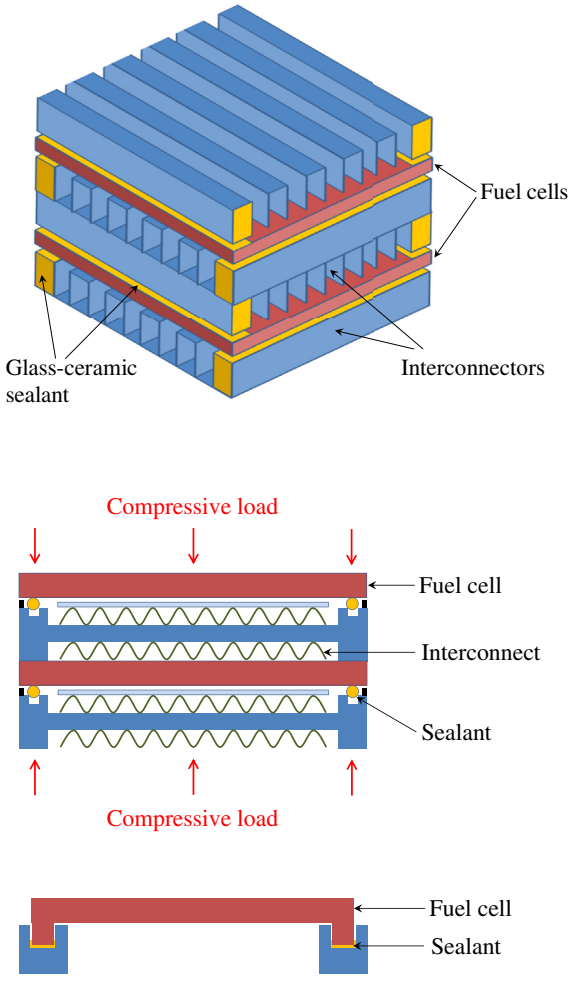

Fig. 1. Typical sealing configurations in planar SOFCs [14–16].

(iii) Chemical inertness with respect to these materials under the stack fabrication and operation conditions.
(iv) Coefficients of thermal expansion (CTE) compatible with those of the electrochemical cell constituents and other construction materials.
(v) High electrical resistivity ($>10^5$ Ohm cm) under operating conditions.
(vi) Minimum volatilization and diffusion of the sealant components.

(vii) No tendencies to bulk reduction, oxidation, hydration, carbonate formation, and reactions with other gaseous species such as SO_x and H_2S.

(viii) Thermal and morphological stability at the cell operation temperatures and during startup/shutdown.
(ix) Compatibility of the characteristic temperatures, primarily T_g, T_c, softening and maximum shrinkage temperature, with the limitations arising from properties of the electrochemical device components and target operation regimes.
(x) Superior thermal shock resistance and high mechanical strength.
(xi) Good sinter ability, easy processing, and an absence of seal defects such as pores, bubbles or micro cracks.

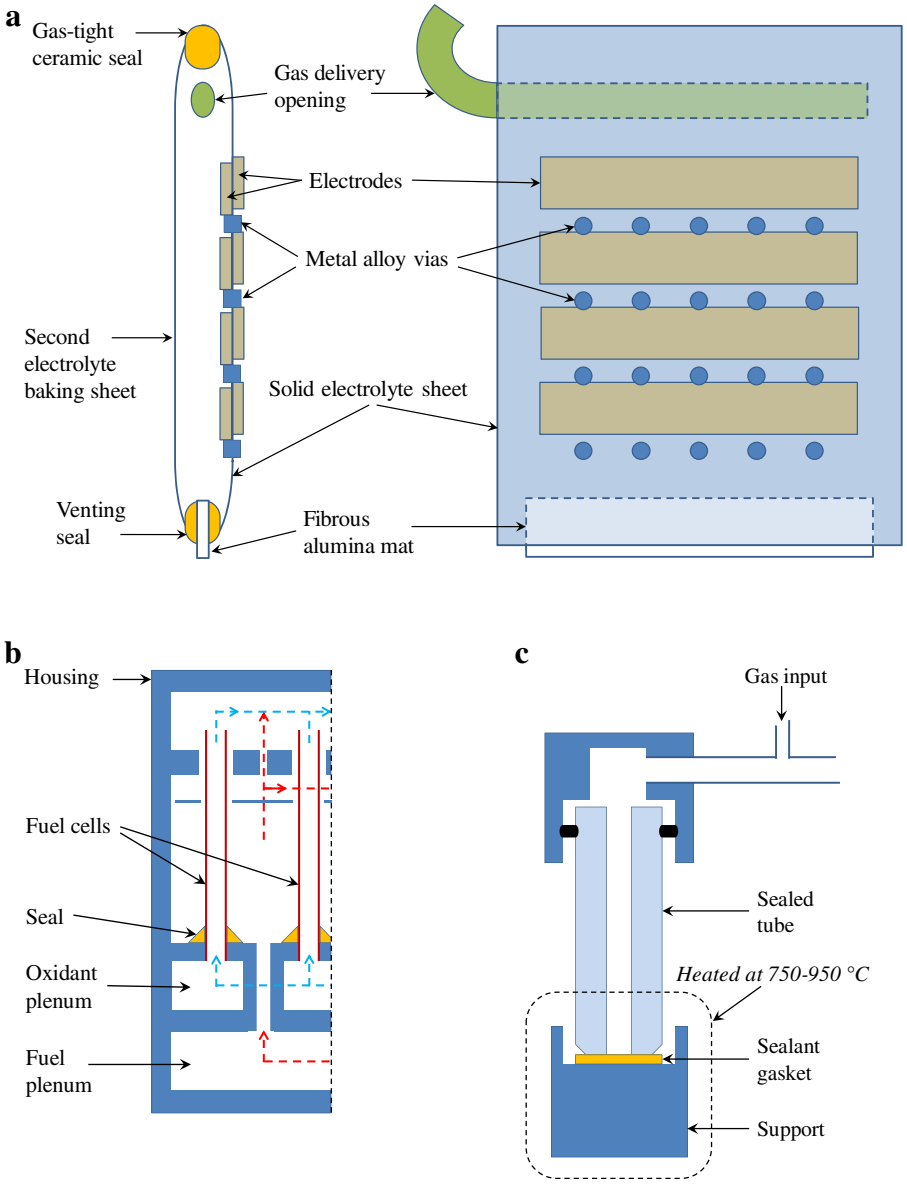

Fig. 2. Examples of seal configurations [17–19]: (a) planar SOFCs; (b) tubular SOFCs; (c) cell for sealant testing.

(xii) Stability with respect to local heating, high applied voltage, flame, carbon deposition and other parasitic phenomena.

(xiii) Self-healing ability originating from viscous flow of the seal glass.

(xiv) Availability of the seal components and low costs.

Many of these requirements are not fully compatible with one another. Moreover, although a number of sealants with attractive properties are already known in the literature, no universal concepts applicable for most types of the electrochemical devices can be found as the entire ranges of operation conditions, cell materials and optimized stack configurations are very large. The developments of novel glass-ceramic sealants with advanced properties are therefore considered among main challenges in this field.

3. Methodological aspects

Sealant is usually applied onto the surfaces of SOFC components using powdered glass mixed with a binder. The glass processing involves the following main steps: (a) weighing and blending of the raw materials, (b) batch calcinations, (c) fusion procedure, (d) casting in the form of monolith pieces (bulk) and/or fritting. In the laboratory scale, batch is usually fused in alumina, zirconia or Pt crucibles in the temperature range 1400–1600 °C, in air. Glasses in bulk form are produced by pouring a melt on preheated metallic molds followed by annealing near the glass transformation range; the glass particulates might be obtained by super cooling of a melt in cold water. Subsequently, fritted glass in the form of irregular granules is dried and milled followed by determination of fine particles sizes and their distribution using light scattering technique.

Fourier transform infrared spectroscopy (FTIR), Raman spectroscopy, magic angle spinning-nuclear magnetic resonance (MAS-

NMR) spectroscopy and other modern spectral techniques were developed and employed to shed a light into the glass structure. In this regard MAS-NMR spectroscopy is apparently the most informative technique that allows determining coordination state of cations in glass structure. For each glass composition a resonance line covers the chemical shift range of cations in several Q^n groups with n ranging from 0 to 4 [24]. Moerover, quantitative Q^n distributions can be obtained by curve fitting and spectral deconvolution [25] as it was demonstrated elsewhere [26]. In our research works [26,27], ^{29}Si MAS-NMR spectra were recorded on a Bruker ASX 400 spectrometer operating at 79.52 MHz (9.4 T) using a 7 mm probe at a spinning rate of 5 kHz. The pulse length was 2 μs and 60 s delay time was used; kaolinite was used as the chemical shift reference. ^{27}Al MAS-NMR spectra were recorded on a Bruker ASX 400 spectrometer operating at 104.28 MHz (9.4 T) using a 4 mm probe at a spinning rate of 15 kHz [26,27], with 0.6 μs pulse length, 4 s delay time, and $Al(NO_3)_3$ as the reference.

The information on thermal and thermo-mechanical properties is usually collected employing differential thermal analysis (DTA), dilatometry and hot-stage microscopy (HSM); important complimentary data may also be obtained employing high-temperature X-ray diffraction (XRD), calorimetry, thermogravimetry and other methods. As an example, in the frame of the experimental trials to synthesize pyroxene based glasses and glass-ceramics [20,28–30] DTA of fine powders was carried out in air at different heating rates varying between 5 and 40 K min^{-1}. The temperature for glass transition (T_g), onset of crystallization (T_c) and peak temperature of crystallization (T_p) obtained from DTA thermographs served as useful indicators for further sintering and crystallization studies. In regard to sintering studies for most of the glasses experiments have been conducted using dilatometric measurements and with the application of low uniaxial pressures [20,28,29]. The dilatometry allows recording continuously the sample contraction; although the presence of the outer tension applied on the sample by the dilatometer rod and the friction between contacting areas affect the sintering kinetics leading to a fictive contraction anisotropy. A standard dilatometer only allows measuring the contraction in one dimension, the detection of anisotropy effect so needs another technique. The hot-stage microscopy (HSM) is a good alternative for studying sintering processes since it permits to follow continuously the contraction process without external charges or friction. If the samples have cylindrical geometry, a common practice in sintering studies, the axial and radial contractions can be simultaneously recorded, and the anisotropy during sintering can be determined [31,32]. For example, a side-view hot-stage microscope (LeitzWetzlar, Germany) equipped with a Pixera video-camera and image analysis system was used in our studies [33,34] for investigation of sintering behavior of glass-powders compacts. The microscope projects the image of the sample through a quartz window and onto the recording device; the computerized image analysis system automatically records and analyzes the geometry changes of the sample during heating. The image analyzer takes into account the thermal expansion of the alumina substrate while measuring the height of the sample during firing, with the base as a reference.

The comparative studies using DTA and HSM under the same heating conditions are very useful in investigating the effect of glass composition on sintering and devitrification phenomena. It is well established that sintering and crystallization processes can occur one after the other or concurrently. Thus, the sintering stage should be completed before crystallization takes place (Fig. 3a) [35]. Final dense and low porosity materials are needed for obtaining a gas-tight glass-ceramic seal. In contrast, if crystallization occurs before sintering is completed (Fig. 3b), the viscosity increases sharply and sintering stops. Under these conditions, a porous glass-ceramic or ceramic material is produced [36].

Quantitative X-ray diffraction (XRD) analysis is crucial in investigating thermal and morphological stability of sealants at the cell operation temperatures [37,38]. For pyroxene based GCs it was performed by combined Rietveld-R.I.R. (reference intensity ratio) method [34,35]. One example is presented in Fig. 4. This technique makes it possible to refine the lattice constants, phase fractions, and coefficients corresponding to sample displacement and asymmetry.

As for the mechanical testing the preference of a three-point bending strength test design relies on fact that this test design is reliable, appropriate and easy in the case of ceramic/glass-ceramic materials. With this design, the test values are easy to compare; however, it must be noted that the results can strongly be affected by the superficial fissures, cracks or defects. Following to the protocol established in our lab, the rectangular bars with dimensions of $4 \times 5 \times 50$ mm^3 were prepared by uniaxial pressing (80 MPa) from the glass powders having mean particle sizes of 10–20 μm [39,40]. For investigating the adhesion and chemical interaction of the glasses with SOFC components, interconnect-glass-electrolyte samples were obtained by sandwiching the glass coated YSZ wafer and the interconnect plate. After sintering at the initial stage, the temperature is to be decreased down to SOFC operating temperature (i.e. 800–850 °C) and maintained constant during 300–500 h. Exhaustive description of the procedures used for the measurements of electrical properties, gas permeation, thermal shock resistance, and interfacial and morphological stability can be found in the experimental works [29,30,33,35].

4. Families of glass and glass-ceramic sealants

The majority of SOFC seal development has focused on bonded, rigid seals; primarily glasses and glass-ceramics (GC), which essentially "glue" the stack components together. The glass seals

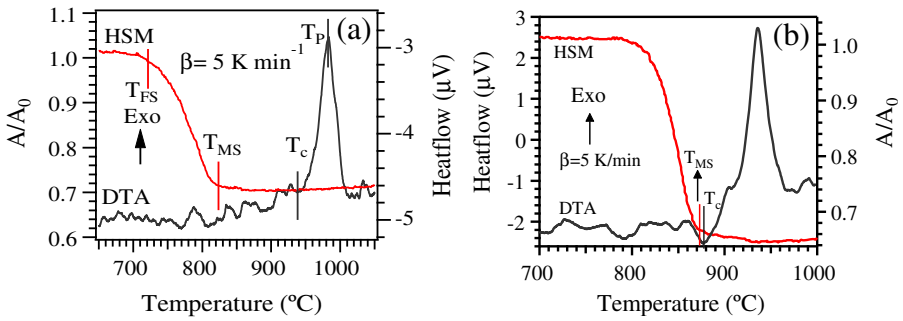

Fig. 3. One example illustrating relationships between the HSM and DTA data at the same heating rate (T_{FS}, first shrinkage; T_{MS}, maximum shrinkage; T_c, onset of crystallization; and T_p, peak crystallization temperature). The data (a) correspond to diopside [35] and (b) corresponds to melilite glass [36] system.

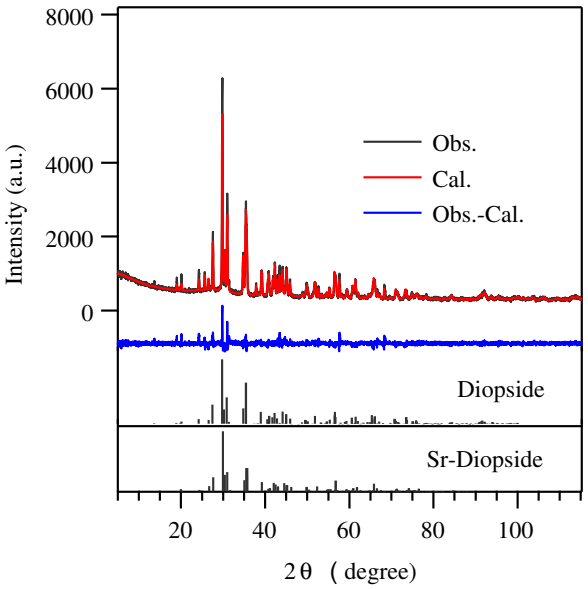

Fig. 4. Observed, calculated, and difference curves from the Rietveld refinement of the 7 mol% SrO doped diopside-Ba disilicate GCs [35].

are designed to soften, and flow above the SOFC operating temperature to provide hermetic seals by mechanical/chemical bonding. On cooling back down to operating temperature, the glass crystallizes to form a rigid, bonded seal. A principal advantage of glass seals is that the glass composition can be tailored to optimize the properties like CTE, mechanical strength, electrical resistance, etc.

Most of the GC based sealants proposed so far are alkali or alkaline-earth aluminosilicate-based; borate based, phosphate based or borosilicate GCs (e.g., [9,41]). However, every material has some advantages which are coupled along with some drawbacks. Alkali silicate glasses or GCs, in principle are not suitable as sealants because alkali cations tend to react with other components of the electrochemical devices [42], form volatile oxides and stable hydroxides and carbonates, and can lead to chromium poisoning. Further, most of the researchers have searched sealing materials on Ba-aluminosilicate GC system and its derivatives [9,42–45]. The majority of these glass compositions contain high amount of BaO (30–35 mol%), leading to the crystallization of monoclinic celsian ($BaAl_2Si_2O_8$) after long-term heat treatments [9] and formation of detrimental crystalline phase $BaCrO_4$ when interfacing with Cr-based metallic interconnect materials in air at operating temperatures [46]. Significant content of BaO may also promote interaction with water vapor, leading to sealant degradation under SOFC operating conditions. For example, Pacific Northwest National Laboratory (PNNL) patented a glass–based sealant named as G18 ($15CaO–35BaO–5Al_2O_3–10B_2O_3–35SiO_2$ (mol %)) [47]; the proneness of G18 glass for crystallizing the low thermal expansion monoclinic $BaAl_2Si_2O_8$ phase during long-term SOFC operation, its high content of BaO that might also react with water vapor and Cr-containing gaseous species (CrO_3 or $CrO_2(OH)_2$) diffused to the glass surfaces to form $BaCrO_4$, constitute the most serious drawbacks as SOFC sealant. The large CTE differences between this chromate ($(18–20) \times 10^{-6}$ K^{-1}), the sealing glass (CTE of $(10–13) \times 10^{-6}$ K^{-1}) and the metallic interconnects ($(11–13) \times 10^{-6}$ K^{-1}) lead to significant losses in bonding strength between SOFC glasses and interconnect materials or to their physical separation.

Also, B_2O_3 forms volatile compounds with water vapor leading to seal degradation [9]. Glasses with B_2O_3 as the only glass former have shown up to 20% weight loss in the humidified H_2 environment and extensive interactions with cell component materials both in air and wet fuel gas [48]. Thus, high amount of B_2O_3 in the sealants is not seen with alacrity. Some P_2O_5-based glasses have also been investigated for sealing purposes. Again, these compositions face a severe problem of volatilization of phosphate component leading to easy crystallization of pyro- or metaphosphates. These phases show poor stability at high temperature in wet fuel gas atmosphere [41,49]. The difficulties in meeting all the requirements in a given material stimulated and many research groups throughout the world are searching for alternative glass sealants [10–12,21–23,38,50–62]. Also In the current review paper an attempt was undertaken to analyze the compositional range and properties of aluminosilicate-based sealants aiming at their further improvements. The next paragraph is focused, therefore, on short excurse in the structure of silicates and aluminosilicates.

4.1. Structural features of silicates and aluminosilicates

Aluminosilicates are the most common minerals owing to the abundance of the silicon and aluminum in the Earth's crust. Different silicates are composed of individual SiO_4^{4-} tetrahedrons which can be either bonded to other cations or linked together through corner oxygens shared with other SiO_4^{4-} groups (Figs. 5–8). Aluminum plays particular role in silicate structures being six- or four-fold coordinated with oxygen and giving rise to the various aluminosilicates. In the latter case $(AlO_4)^{5-}$ groups substitute for SiO_4^{4-} while charge balancing is being satisfied by cations of alkali (Li, Na, K), alkaline-earth (Be, Mg, Ca) or transition (Fe, Mn, Ti, Zr, etc.) metals.

SiO_4^{4-} tetrahedrons shared with octahedral groups are basic units of nesosilicates (island silicates) also known as orthosilicates (Fig. 6a). This combination is possible due to matching edge sizes of isolated SiO_4^{4-} tetrahedrons (2.64 Å) and octahedral groups that contain relatively small cations likeMg^{2+}, Fe^{2+}, Zr^{4+}, etc. (Fig. 6a). Zircon ($ZrSiO_4$), forsterite (Mg_2SiO_4), fayalite (Fe_2SiO_4), monticellite ($CaMgSiO_4$) are some representatives of nesosilicates.

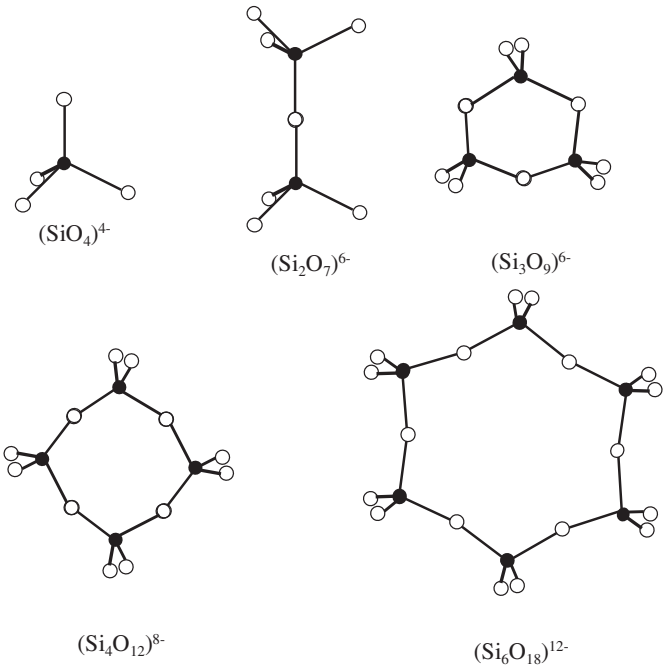

Fig. 5. The simple tetrahedron and complicated groups built from [SiO_4] tetrahedrons.

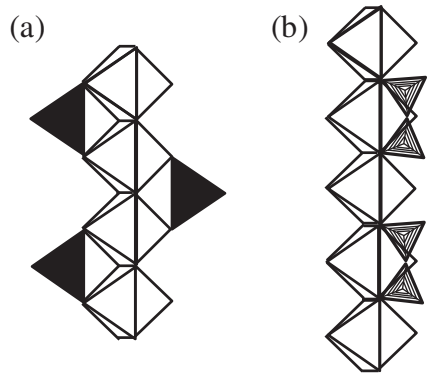

Fig. 6. The elements of silicates structure: (a) orthogroups of [SiO_4] tetrahedrons; (b) diorthogroups of [Si_2O_7].

Diorthogroups $Si_2O_7^{6-}$ are formed through sharing of corner oxygens from tetrahedrons are basic units of silicates referred to sorosilicate group. $Si_2O_7^{6-}$groups feature dimensions (4.1–4.2 Å) comparable with the edges of octahedral groups formed by larger cations like Ca^{2+}, Sr^{2+}, Ba^{2+}, etc. (Fig. 6b). One good example of sorosilicates is minerals from melilite family, in particular akermanite $Ca_2MgSi_2O_7$ that forms continuous solid solutions along with gehlenite $Ca_2Al_2SiO_7$.

Cyclosilcates (ring silicates) are composed of several SiO_4^{4-} tetrahedrons that shared oxygens in a ring structure creating $Si_3O_9^{6-}$, $Si_4O_{12}^{8-}$, $Si_5O_{15}^{10-}$ and $Si_6O_{18}^{12-}$ groups (Fig. 5). Some examples of cyclosilicates are cordierite – $Mg_2Al_3AlSi_5O_{18}$ and beryl – $Be_3Al_2Si_6O_{18}$. Inosilicates (single chain silicates) are formed when SiO_4^{4-} tetrahedrons shared oxygens in a way to create long single chains with the basic structural units SiO_3^{2-}or $Si_2O_6^{4-}$. Minerals from pyroxene group such as the enstatite $MgSiO_3$ or diopside $CaMgSi_2O_6$, wollastonite $Ca_3Si_3O_9$, rhodonite $Mn_5Si_5O_{15}$ [63] are representatives of single chain silicates (Fig. 7). Inosilicates with double chain structure (the basic structural units $Si_4O_{11}^{6-}$) are formed from two chains of SiO_4^{4-} tetrahedrons linked together in a way to share three of oxygens from each tetrahedral group.

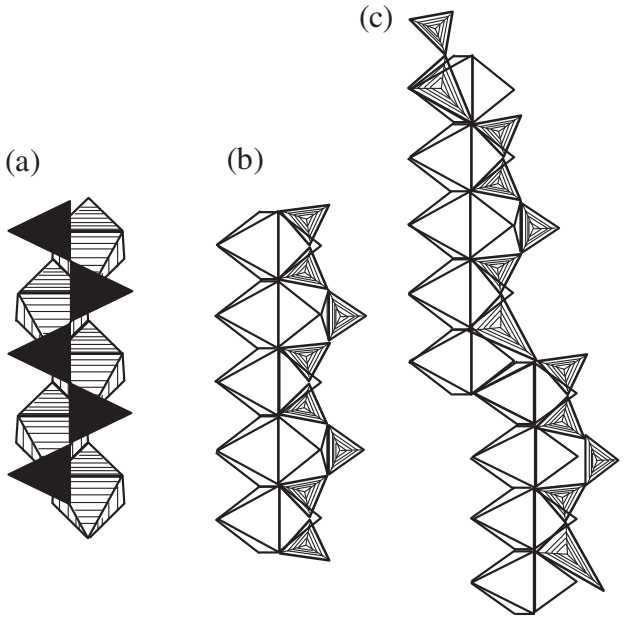

Fig. 7. Structure of some inosilicates (single chain silicates): (a) diopside – CaMg[Si_2O_6]; (b) wollastonite – $Ca_3[Si_3O_9]$; (c) rodonite – $Mn_5[Si_5O_{15}]$.

Phyllosilicates (sheet silicates) are composed of tetrahedrons that join together in form of sheets. Thus, in the clay minerals three of the four oxygens in each tetrahedron are shared with other tetrahedrons giving a continuous sheet as shown in Fig. 6. Three of four oxygens in every tetrahedron are valency-satisfied. As the fourth oxygen is only bonded to one Si, the silica layer can join cations of similar structures like gibbsite layer. The basic formula of silica sheets is therefore $(SiO_{2.5})^-$ or $(Si_2O_5)^{2-}$. Apart of clay, minerals micas, talc, serpentines, etc. belong to sheet silicates.

In tectosilicates (framework silicates) like quartz and in its polymorphs (tridymite and cristobalite) each SiO_4^{4-} tetrahedron shares the corner oxygens with other four tetrahedrons. Likewise feldspars are the framework silicates in which Al^{3+} can substitute for some Si^{4+} ions resulting in different arrangements of Na^+, K^+ and Ca^{2+}cations within the framework structure to achieve charge balance.

4.2. Aluminosilicate-based glass and glass-ceramic sealants

The thermodynamic properties of aluminosilicate glasses are mainly determined by their composition and the network connectivity. When introducing Al_2O_3 in the fully connected corner-sharing tetrahedral network of amorphous silicates, the Al atoms substitute for the Si atoms in the center of the tetrahedra thus leading to charged $(AlO_4)^{5-}$ units. In order to maintain local charge neutrality, $(AlO_4)^{5-}$ units can be charge-compensated by alkali cations (K, Li) which must be present in the vicinity of each such tetrahedron. Therefore, the $(AlO_4)^{5-}$ tetrahedra substitute directly into the network for silicon–oxygen tetrahedra, and simultaneously tend to suppress the immiscibility while raising the T_g and decreasing the CTE of glasses [64,65]. However, if the concentration of these cations becomes larger than needed for a full compensation of the $(AlO_4)^{5-}$ units, then the cations play the role of modifiers. Namely, these create non-bridging oxygens (NBO) by breaking T–O–T linkages (T = Si/Al) and/or play the role of charge balancing, by neutralizing the AlO_4 entities.

Considering above mentioned features, alkali or alkaline-earth oxides such as Na^+, K^+, Ca^{2+}, Mg^{2+}, Sr^{2+}, Ba^{2+} etc., can serve both as charge compensators and/or as network modifiers in aluminosilicate glasses. These cations perturb silicate frameworks linked by bridging oxygen (BO) and by forming non-bridging oxygens (NBO), which play essential roles in many dynamic properties of melts. In principle, the number of NBO atoms in a glass is directly related to the viscosity of the glass forming liquid [66]. The types of cations in oxide glasses certainly can cause different states of disorder depending on their characteristics, such as ionic radius, charge, field strength, and on their local environments.

4.2.1. Alkali containing aluminosilicate glass/glass-ceramic sealants

Alkali oxides involved in the batch as a modifier contribute to get homogeneous melt at moderate temperatures, to decrease the glass transition temperature, to adjust glass viscosity and to improve the wettability of glasses. Chemical compositions of some alkali containing glasses employed as sealants in SOFC are summarized in Table 1 [21,22,67–74]. Alkali alkaline-earth aluminosilicate seal glasses generally contain 20–45 mol% of network modifiers with the molar ratio $(Na_2O+K_2O)/(CaO + MgO)$ varied in the range 0.03–1.8. Recently Coillot et al. [70] reported on alkali aluminosilicate glasses free from alkaline-earth oxides. Properties of some alkali containing aluminosilicate glass sealants are shown in Table 2 [21,22,67–75]. Values of T_g (545–780 °C) and T_s (680–740 °C) were obtained when Na_2O introduced in the amount of 1.3–18 mol% whilst 7 mol% K_2O containing glasses demonstrated T_g of 470 °C and T_s of 530 °C [21]. Substitution of 5 mol% of Na_2O for SiO_2 in calcium aluminosilicate glass reduced T_g and T_s by 35 and

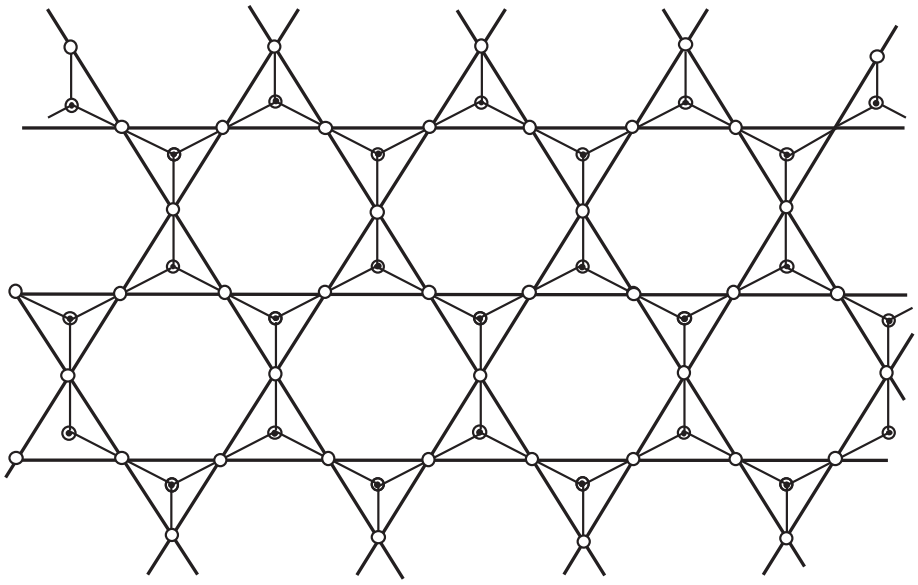

Fig. 8. $[Si_2O_5]_n^{2n-}$ tetrahedral silica layer.

60 °C, respectively, and also increased CTE from 9.2×10^{-6} up to 11.2×10^{-6} K^{-1} [72]. On the other hand, the substitution of 15 mol% Na_2O for SiO_2 in calcium aluminosilicate glasses was found to increase T_g and T_s by 92 °C and 120 °C respectively, whilst CTE decreased from 8.9×10^{-6} down to 8.2×10^{-6} K^{-1} [67]. Values of T_g (468–630 °C) and T_s (540–692 °C) were obtained in Na_2O (7.3–13 mol%) and K_2O (4–10 mol%)-containing glasses [68–70]. Additionally, lowest values of T_g and T_s were revealed when low-field strength K^+ ion was incorporated in silicate glasses. Generally, it is well known that incorporation of alkali ions at the expense of glass formers resulted in disruption of silicate network owing to the increasing number of NBO. Fewer changes in silicate network will occur when alkali ions substitute for alkaline-earth ions. Nevertheless, network disorder increases with growing (Na_2O + K_2O)/(CaO + MgO) molar ratio causing T_g and T_s diminishing (Fig. 9). Consequently, with increasing (Na_2O + K_2O)/(CaO + MgO) molar ratio T_g decreases from 780 to 562 °C and T_s from 740 to 600 °C.

Fig. 10 shows the variation in CTE of alkali containing alkaline-earth aluminosilicate glasses with respect to (Na_2O + K_2O)/(CaO + MgO) molar ratio. CTE of glasses increased from 7.8 to 10.7×10^{-6} K^{-1} when (Na_2O + K_2O)/(CaO + MgO) ratio changes in the range 0 to 0.4, and then decreased down to about 8.2×10^{-6} K^{-1}. CTE values are stabilized with the further increase in (Na_2O + K_2O)/(CaO + MgO) molar ratio, between 0.6 and 1.7. This anomalous behavior can be explained on the basis of mixed modifier ions presence and their distribution in the glasses. When mixing the high- and low-field strength cations (e.g., Mg^{2+} and K^+, respectively) to the aluminosilicate, the high field-strength cation is

Table 1
Some alkali alkaline-earth aluminosilicate glass compositions (%) investigated for SOFCs.

	Na_2O/K_2O	CaO/MgO/BaO	Al_2O_3	SiO_2	Others	Ref.
mol	10–25	15.0	10.0	45–60	5.0 TiO_2	[67]
wt	9.6–23.8	12.9–13	15.7	41.5–55.6	6.1–6.2 TiO_2	
mol	7.3/10	3.34/–/8.23	2.80	66.9	1.43	[68,69]
wt	6.2/13	2.6/–/17.4	3.9	55.4	1.43	
wt	–/5–10	–/–/10–15	0–15	20–25	5–10 ZnO 45–50 Bi_2O_3	[21]
mol	13/4	–	–	65–75	0–10 B_2O_3 1 La_2O_3 7 ZrO	[70]
wt	11.6/5.4 11.7/5.5	–	–	56–65.5	0–10 B_2O_3 4.7 La_2O_3 12.4 ZrO	
mol	9–12	24–26	16–18	53–58	–	[22,71,72]
wt	9.4–11.3	20.4–22.1	24.8–27.8	48.4–52.8	–	
mol	1.3 6.2 1.3	39.7/0.5 40.9/– 36.8/0.4	13.4 11.2 12.4	45 36 41.8	– 1La_2O_3/4.7ZnO 7.3 ZnO	[71]
wt	1.3 5.7 1.2	34.8/0.3 34.2/– 31.6/0.27	21.4 17.1 19.4	42.2 32.3 38.4	– 5La_2O_3/ 5.7ZnO 9.1 ZnO	
mol	10–12.1	22.2–25.6	6.1–7.3	51.7–57	8–10	[75]
wt	10–12	20–23	10–12	50–55	8–10	
mol	18–23	18	9	40–45	10 B_2O_3	[72]
wt	17.3–22.1	15.6–15.7	14.2	37.2–42	10.8 B_2O_3	

Table 2
Properties of some aluminosilicate glass and glass-ceramic compositions.

T_g, °C	T_s, °C	T_p, °C	Density (g cm^{-3}): glass/GC	CTE (10^{-6} K^{-1}): glass/GC	Ref.
Alkali alkaline-earth silicate					
562–654	589–709	T_{p1}: 705–831 T_{p2}: 864–965	–	8.19–8.88/8.27 (200–550)	[67]
468–486	540–600	–	–	11	[68,69]
470–480	530–575	–	–	9.41–11.2 (50–460)	[21]
610–630	675–692	–	–	7.5–8.3	[70]
670	740	T_{p1}: 830 T_{p2}: 940	–	–/10.7	[22,73,74]
700–780	–	T_{p1}: 780–1020 T_{p2}: 900	–	7.8–9.7(200–400)/ 10 (RT–800)	[71]
670	740	–		9.4–9.8 (300–500)/ 10.7 (RT–800)	[75]
545–580	680–740	–		9.3–11.2 (200–400)	[72]
Alkaline-earth silicate					
730	750	–	–/3–3.10	11.2	[120]
619	682	–	–	10.5 (RT–500 °C) 11.8 (200–800 °C)	[37,38,82,83]
666–699	–	780–833	–	8–8.3	[84]
627–730	657–765	844–903	–	7.9–8.3 (200–600)	[85]
645	693	–	–	11.76/11.68	[86]
685	741	–	–	11.87/11.63 (RT–680)	[87]
630	685	–	–	11.80/12.40 (RT–630)	[87]
685	741	–	–	11.6/11.9 (RT–T_s)	[88]
712–800	748–838	–	3.6–4.19	8.4–10.7/8.5–10.1	[89]
584–650	–	779–789	–	11.4–13/12–13	[90]
640–722	664–745	T_{p1}: 820–890 T_{p2}: 860–930	3.6–3.8	10.5–11.5 (200–650)	[91]
635–653	673–683	730	–	9.9–11.8/11.3–12.5 (30–500)	[92]
611–672	660–712	720–785	3.89	9.9–12.4 (RT–610)	[42]
Boron-containing alkaline-earth silicate					
678–718	701–748	775–858	3.69–3.86	–/9.1–10.8 (100–650)	[93]
710–724	–	760	–	7.94–8.06/8.05–8.43	[114]
690–720	–	807–825	3.4–3.8	7.5–8.5	[94]
650–690	–	766–1074	–	6.84–7.71/7.67–8.10	[95]
620	620–735	–	–	4.7–7.76	[96]
554–659	660–709	T_{p1}: 821–913 T_{p2}: 1092–1021	2.67–3.32	8.29–9.72	[97]
775	815	965	–	10.8	[98]
635–775	670–815			10.8 (50–775)	[99,100]
668	745	T_{p1}: 820 T_{p2}: 864	–	9–12/11	[23,101–103]
–	645–781	655–745	–	9.23–11.17 (200–650)	[104]
595–620	–	760–808	3.4–3.8	–/9.5–13.2 (100–750)	[105]
–	912–937	–	3.24–4.54	4.1–8.1	[106]
601–622	–	T_{p1}: 762–838 T_{p2}: 896–907		10.34–10.83	[107]
–	656–854	–	2.61–3.92	4.92–10.98	[108]
631	662	–	–	9.9 (RT–630)	
575–633	628–685	–	–	11.2–11.8 (RT–630)/10.8–12.5 (RT–1000)	[44]
Others					
655	–	790	–	–	[58]
576	–	–	–	9.4	[109]
552	558	–	–	11.9 ((275–550)/10.1–13.0	[110]

consistently favored to form the NBO's while low-field-strength ions behave as charge compensators. On the other hand, when pair of cations with the similar ionic radii but different charges (e.g., Ca^{2+} and Na^{+}, respectively) is mixed, the charge difference apparently plays an important role in the preference to the formation of dissimilar pairs primarily in order to maximize a homogeneous distribution of charges in the glasses. Nonrandom distributions of modifying cations in Ca-Na silicate glasses due to the similar ionic radii affect the dynamics of Na^{+} and related properties in the glass [76,77]. The desired CTEs, $(9–11) \times 10^{-6}$ K^{-1}, have been obtained when the glasses featured $(Na_2O + K_2O)/(CaO + MgO)$ ratio in the range 0.1–0.5 (Fig. 10).

As a matter of fact, most of the glass/glass-ceramic candidates investigated up to now contain no alkalis and the impact of alkali appears unclear. Some alkali metal-containing glasses used for sealants in SOFC enhance the chromium vaporization from metallic interconnects by the formation of very volatile Na_2CrO_4 and K_2CrO_4 species [9]. Chou et al. [68,69] discussed the compatibility between

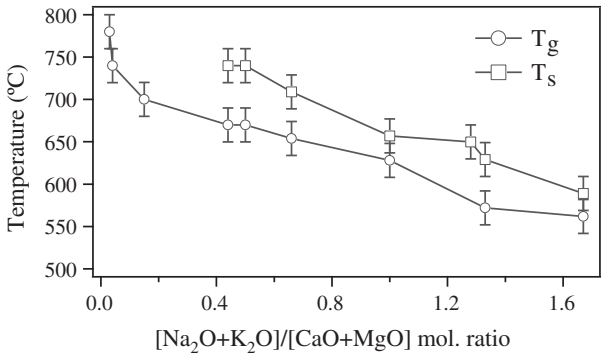

Fig. 9. Variation of glass transition (T_g) and glass softening point (T_s) with respect to ($Na_2O + K_2O$)/(CaO + MgO) molar ratio in some alkali alkaline-earth aluminosilicate glass compositions (see Tables 1 and 2).

Crofer22APU interconnects and potassium oxide containing glasses. The addition of K_2O in the parent glass sealant led to debonding of the sealant from Crofer22APU due to alkaline-earth chromates formation. No discussion about corrosion mechanism, like alkali chromates formation and their volatility, on as-received Crofer22APU has been presented. Kaur et al. [67] studied the microstructure at the interfaces of Crofer22APU and glass with varying Na_2O content from 10 to 25 mol%. The diffusion couple between Crofer and glass (10 mol% Na_2O) was found to show a good and smooth interface; no traces of Na^+ were observed. Several investigations [22,67,68,70] stated that alkalis role is still unclear, and thus their drawbacks may be smaller than expected and it may be advantageous to keep them in glass seal composition. For instance, Smeacetto et al. [74] have extensively studied alkali containing alkaline-earth aluminosilicate glasses and found that glasses containing a low amount of sodium oxide can be used as sealing material for SOFCs. Further, Smeacetto et al. [74] have also evaluated the performance of Na_2O-containing GC sealant in two SOFC short stack configurations. The glass-ceramic sealant was reported to have a good chemical and thermo-mechanical compatibility with both Crofer22APU and yttria-stabilized zirconia (YSZ) components. At the same time, one should note that potential effects of Na^+ presence are not limited to the GC|YSZ and GC|interconnect interfaces. In particular, high surface diffusivity of Na^+ may cause poisoning of the electrodes; sodium incorporation in the solid electrolyte grain boundaries may lead to worse mechanical strength and, often, higher electrical resistivity of stabilized zirconia (e.g., [4,78] and references cited). These effects associated with a slow degradation in the SOFC performance with time cannot be ignored in the seal developments and require long-term testing of such sealants.

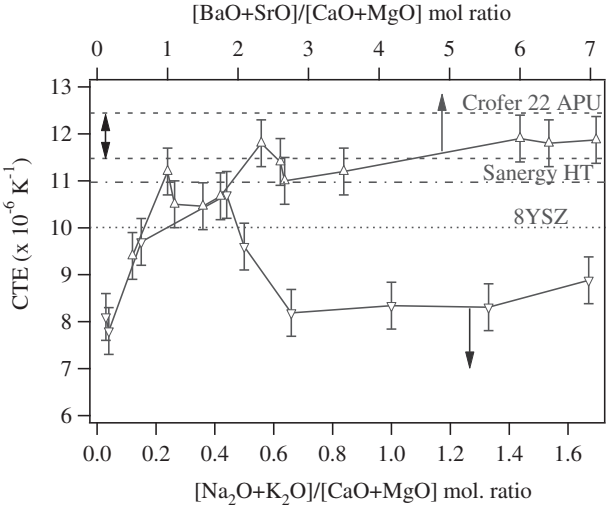

Fig. 10. Variation of the coefficients of thermal expansion (CTE) as function of the ($Na_2O + K_2O$)/(CaO + MgO) molar ratio in some alluminosilicate glass compositions and (BaO + SrO)/(CaO + MgO) ratio in alluminosilicate compositions investigated for SOFCs (based on the data from Tables 2, 3 and 4).

4.2.2. Alkaline-earth aluminosilicate glass/glass-ceramic sealants

A number of alkaline-earth aluminosilicate glasses sealants have been apprised for SOFCs and other solid-electrolyte devices. Knowing the fact that alkaline-earth metals have different chemical properties such as field strength, ionic radius, and electro negativity those can have strong influence on T_g, T_s, CTE, crystallization behavior, electrical conductivity as well as the reactivity of glasses. To date, the most well-known systems that have been widely used for sealing applications are the BaO/SrO–Al_2O_3–SiO_2–based, BaO/SrO–CaO–Al_2O_3–SiO_2-based and BaO/SrO–CaO/MgO–Al_2O_3–SiO_2-B_2O_3-based glass systems. Some compositions of alkaline-earth and boron-containing aluminosilicate glasses employed as sealants in SOFCs are summarized in Tables 3 and 4 whilst their properties are provided in Table 2 [23,37,38,42,44,58,79–113]. Relatively wide ranges of T_g, T_s and CTE were obtained in the alkaline-earth containing boron/alumino silicate glasses. Those are as follows:

(i) For MgO-containing glasses T_g varied in the range of 620–700 °C, T_s changed between 620 and 735 °C, and CTE varied in the range of (4.7–8.1) × 10^{-6} K^{-1}[96].
(ii) For CaO-containing glasses T_g varied in the range of 710–724 °C, T_s is close to740 °C, and CTE changed in the interval 7.9 × 10^{-6} to 8.1 × 10^{-6} K^{-1} [114].
(iii) For SrO containing glasses T_g varied in the range of 660–800 °C, T_s changed in the range of 660–838 °C and CTE varied in the range of (6.8–11.5) × 10^{-6} K^{-1} [89,91,94,98,99,115,116].
(iv) Finally for BaO-containing glasses T_g varied in the range of 601–789 °C, T_s changed in the interval 656–937 °C, and CTE was (4.1–11.8) × 10^{-6} K^{-1} [84,85,95,107,108,117].

Barium-containing aluminosilicate glasses demonstrated lowest T_g and T_s (Table 2) and highest CTE values (Table 2) as compared to other alkaline-earth containing glasses, for instance CaO and SrO containing glasses. This behavior can be explained on the basis of field strength values. The field strength of alkaline-earth modifier cations fallows the fallowing trend: Mg^{2+} (045–0.51) > Ca^{2+} (0.33–0.35) > Sr^{2+} (0.27) > Ba^{2+} (0.24). Since the force characteristic of Mg^{2+} cations is highest among alkali and alkaline-earth cations and lowest among network-former ions, one can assume that the Mg^{2+} cations in the glass network can exist as both modifiers and network formers. CTE increased with increasing BaO contents from 20 to 40 mol% and achieved a maximum of approximately 11 × 10^{-6} K^{-1} at 40 mol% BaO in the BaO–Al_2O_3–La_2O_3–SiO_2–B_2O_3 system [118,119]. CTE also increased with increasing SrO content, with a maximum of 9.7 × 10^{-6} K^{-1} at 25.7 mol% SrO in the SrO–Al_2O_3–La_2O_3–SiO_2–B_2O_3 system [97]. However, increasing SrO and decreasing B_2O_3/SiO_2 ratio resulted in growing of the glass transition temperature (T_g) and softening temperature (T_s) as the structure becomes inverted and rigid [97]. Hence, the CTE increases directly with the decreasing the field strength of alkaline-earth cations due to the weaker bonding at lower field strength.

However, the effect of the network modifier on the CTE, T_g and T_s of a seal glass is complex and is related to the field strength, to the

Table 3
Some alkaline-earth aluminosilicate glass compositions (%) investigated for SOFCs.

	CaO	SrO/BaO	Al_2O_3/La_2O_3	SiO_2	B_2O_3	Others	Ref.
mol	26.48	26.48/–	1.96	41.16	1.92	2 TiO_2	[79]
wt	20.6	38.1/–	2.8	34.4	1.9	2.2 TiO_2	
mol	23.4	23.4	–	39.6	3.6	10 ZnO/10 MnO_2/10La_2O_3	[80]
wt	13.6–18.3	25.2–33.8	–	24.7–33.1	2.6–3.5	11.3 ZnO/12 MnO_2/33.9La_2O_3	
mol	19.2	18.5	2.9	42.2	1.9	13.2 ZnO/2.1 TiO_2	[81]
wt	15	26.6	4.1	35.2	1.8	14.9 ZnO/2.3 TiO_2	
mol	15	–/35	5	35	10	–	[37,38,
wt	8.8	–/56.4	5.4	22.1	7.3	–	82]
mol	–	–/30	–	40	0–7.5	20 ZnO 2.5–10 Mn_2O_3	[84]
wt	–	–/45.1–48.2	–	23.5–25.2	0–5.5	15.9 –17.0ZnO 4.1–15.5 Mn_2O_3	
mol	–	–/30	0–10	40	0–10	20 ZnO	[85]
wt		–/47.7–49.3	0–10.6	24.9–25.8	0–7.5	16.9–17.5 ZnO	
mol	5	43.5 ($SrCO_3$)	–	34	10	5 Y_2O_3 2.5 ZnO	[86]
wt	2.6	59.6	–	19	6.5	10.5 Y_2O_3 1.9 ZnO	
mol	6	42.5	–	37.0	8.5	6 Y_2O_3	[87]
wt	3.8	49.4	–	25	6.6	15.2 Y_2O_3	
mol	15	–/35	5	35	10	–	[87]
wt	8.8	–/56.4	5.4	22.1	7.3	–	
mol	–	20–40	4–12.5	34–48	–	6–29 ZnO 3–10 TiO_2	[89]
wt	–	19.05–46.21	2.82–12.98/7.45–24.8	14.52–28.17	–	4.24–25.89 ZnO 13.01–33.42 TiO_2	
mol	–	18.5–20/30–33.3	4.6–5/4.6–5	27.7–30	9.2–10	0–1.8 P_2O_5	[90]
wt	–	16.5–18.3/44.1–40.7	4–4.5/12.9–14.4	14.4–15.9	5.5–6.2	0–2.2 P_2O_5	
mol	–	38.8	–	52.5	–	8.7 ZnO	[91]
		39.5	–	40.1	11.5	8.9 ZnO	
		38.8	–	40.9	9.4	9.1ZnO/1.8V_2O_5	
		40.5	2.4	41.0	5.9	9.1ZnO/1.1Cr_2O_3	
wt	–	51	–	40–*X*	0–10	9 ZnO *X* = 4V_2O_5, 3Al_2O_3, 2Cr_2O_3	
mol	21.6	–/18.3	0.5	59.6	–	–	[111]
wt	15.8	–/36.7	0.7	46.8	–	–	
mol	15	–/35	5	32–37	8	0–5 P_2O_5	[92]
wt	8.5–8.9	–/54.2–56.5	5.1–5.4	19.4–23.4	5.6–5.9	0–7.2 P_2O_5	

amount of a network modifier, and also to the presence of other concomitant components in the glass. Thus:

(i) T_g of 575–668 °C, T_s of 558–781 °C and CTE range (9.9–12.0) × 10^{-6} K^{-1} were revealed for CaO–BaO-containing glasses [23,37,38,42,82,83,92,101–103].
(ii) T_g of 630–735 °C, T_s of 721–768 °C and CTE of (11.2–12.1) × 10^{-6} K^{-1} are found for CaO–SrO containing glasses [88,120].
(iii) T_g of 584–650 °C and CTE in the range of (11.4–13.0) × 10^{-6} K^{-1} are characteristic of SrO–BaO-containing glasses [90];
(iv) T_g range of 624–715 °C, T_s of 665–750 °C and CTE of (8.6–10.1) × 10^{-6} K^{-1} were obtained for MgO–BaO-containing boron-aluminosilicate glasses. BaO and SrO as modifiers increase the CTE as compared to CaO and MgO due to their low-field strength values [96]. The lowest T_g of 584 °C and highest CTE of 13 × 10^{-6} K^{-1} were obtained for 18.5 mol% SrO and 33.3 mol% BaO-containing aluminosilicate glasses [90].

Fig. 11 displays the variation in T_g and T_s as function of the (BaO + SrO)/(CaO + MgO) molar ratio. These variations are rather discontinuous: (i) when the ratio (BaO + SrO)/(CaO + MgO) ranges from 0.50 to 2.67 T_g and T_s vary in the intervals of 575–650 °C and 640–750 °C, respectively; (ii) T_g and T_s both show an abrupt decrease at the molar ratios from 2.67 to 3.5; (iii) continuous increase in T_s and T_g were observed in the interval 3.5–6; and finally, (iv) significant increase of T_g and T_s were revealed when the molar ratio ranged from 6.50 to 7.08. A general trend to growing CTE has been observed with increasing molar ratio (BaO + SrO)/(CaO + MgO), Fig. 10.

Highly suitable values of T_g, T_s and CTE have been achieved in the barium-containing boron-aluminosilicate glasses (Table 2). However, poor thermal stability and unwanted chemical interaction with the SOFC components limit the application of BaO- and B_2O_3-containing glasses. B_2O_3 works well for decreasing the viscosity of the glass but at the same time it decreases seal thermal stability owing to lowering network connectivity. On the other hand, the compositions that contain large amounts of boron can react in overtime with water vapor and produce gaseous $B_2(OH)_2$ or $B(OH)_3$. This can decompose the seal glass and limit the life span. Notice that Zhang et al. [81] discussed the borate volatility issues in their report.

Glass-ceramics (GCs), formed by the controlled crystallization of glasses, exhibit superior properties with respect to glasses. The performance of GCs can be controlled by proper controlling of the nature and amount of crystalline components. Crystallization typically increases the strength and CTE [102,103]. The higher CTEs of GCs are however entirely consistent with the relative CTE variations of the crystalline phases developed in the glasses. The resultant CTE can be estimated using the standard additive rule $\alpha = \Sigma m_i\alpha + a$ where α is the CTE of the glass-ceramics, m_i and α are the mole fraction and CTE of each phase present in the matrix, respectively, and a_i is a constant factor for phase i [121]. Significant content of BaO in the aluminosilicate glasses can lead to formation of the following crystalline phases: (i) barium silicate ($BaSiO_3$; CTE (9–13) × 10^{-6} K^{-1}), (ii) Barium orthosilicate ($BaSi_2O_5$; CTE ≈ 14 × 10^{-6} K^{-1}), (iii) hexacelsian ($BaAl_2Si_2O_8$; CTE = (7–

Table 4
Boron-containing alkaline-earth aluminosilicate glass compositions (%) investigated for SOFC.

	CaO/MgO	SrO/BaO	Al_2O_3/La_2O_3	SiO_2	B_2O_3	Others	Ref.
mol	–	23.7	–/2.4	52.3	22.6	–	[93]
		16.6	–/2.6	56.4	24.4		
wt	–	30	10	40	20	–	
		30	10	40	20		
mol	30	–	–	40	20	10 Y_2O_3/10 La_2O_3	[114]
wt	21.7	–	–	31.1	18	29.2 Y_2O_3/37.3 La_2O_3	
	19.3			27.5	15.9		
mol	–	–/30	–	40	20	10 Al_2O_3/10 Y_2O_3/10 La_2O_3	[94]
wt	–	–/48.9	–	25.5	14.8	10.8 Al_2O_3	
		–/43.2		22.6	13.1	21.2 Y_2O_3	
		–/39.5		20.6	11.9	28 La_2O_3	
mol	–	30	–	40	20	10 Al_2O_3/10 Cr_2O_3/10 Y_2O_3/10 La_2O_3	[95]
wt	–	39.2	–	30.3	17.6	12.9 Al_2O_3	
		36.9		28.5	16.5	18.0 Cr_2O_3	
		33.9		26.2	15.2	24.6 Y_2O_3	
		30.6		23.6	13.7	32.1 La_2O_3	
mol	–/30	–	–	40	20	10 Al_2O_3/10 Y_2O_3/10 La_2O_3	[96]
wt	–/20.1	–	–	39.9	23.1	16.9 Al_2O_3	
	–/16.6			33.1	19.2	31.1 Y_2O_3	
	–/14.6			29.1	16.9	39.4 La_2O_3	
mol	–	7.9–25.7	12.1–13.1/3.8–4.1	40.9–44.4	12.8–35.3	–	[97]
wt	–	10–30	15/15	30	10–30	–	
mol	–	13.3	13.3/13.4	25–60	0–35	–	[100,112]
wt		12.5–12.9	12.3–12.7/39.5–40.8	13.6–33.7	0–22.1	–	
mol	0–15	–/0–40	0–10/0–15	0–40	0–15	0–5 (ZrO_2)	[23,101–103]
wt	0–6.9	–/0–50.7	0–8.4/0–40.4	0–19.9	0–8.6	0–5.1	
mol	16–24	–/16–24	6/6	30–42	10–14	–	[104]
	–	36–44/–	5/5	30–30	13–16		
	16	16–28/–	5/5	31–43	15		
wt	9.5–13.3	–/26.1–36.5	6.1–6.5/	17.9–26.8	6.9–10.4	–	
	–	40.4–47.4/–	19.4–20.8	18.7–26.7	9.8–11.6		
	10.1–10.8	19.9–32.8/–	5.3–5.5/	21.1–31	11.8–12.5		
			16.9–17.6				
			5.8–6.1/				
			18.4–19.6				
mol	–	–/47.62	4.76	26.67	20.95	–	[113]
wt	–	–/67.3	4.5	14.8	13.4	–	
mol	–	–/40	0–10	33.3–40	16.7–20	–	[107]
wt	–	–/59.5–61.8	0–9.9	19.4–24.2	11.3–14	–	
mol	–	–/12.62–50	5–7.59	15–63.2	16.67–30	–	[108]
wt		–/25.2–68.7	4.6–10.1	8.1–49.5	15.2–18.7	–	
mol	–	20/20	–	40	20	–	[81]
wt	–	23.2/34.3	–	26.9	15.6	–	
mol	10–15	–/32.5–35	2.5–5/0–5	30–39	10–15	–	[44]
wt	6–8.8	–/47.3–56.4	2.4–5.4/0–15.5	19.4–23.2	6.9–11.3	–	

8) $\times$ 10^{-6} K^{-1}), (iv) monocelsian ($BaAl_2Si_2O_8$; CTE = (2–3) $\times$ 10^{-6} K^{-1}), and (v) orthocelsian ($BaAl_2Si_2O_8$; CTE = (7–8) $\times$ 10^{-6} K^{-1}) [9]. The activation energy for crystal growth is very low for the BaO-containing glass (206–300 kJ mol^{-1}) as compared to CaO-containing (413 kJ mol^{-1}) and MgO-containing (340–420 kJ mol^{-1}) aluminosilicate glasses, and thus causes rather poor thermal stability [30, 122]. Consequently, due to low activation energy there is a strong tendency for celsian formation in BaO-containing glasses. The celsian ($BaAl_2Si_2O_8$) crystalline phase having a low CTE value reduces thermal expansion of the resultant GCs. On the other hand, significant content of BaO in the glasses can also lead to formation of $BaCrO_4$ on the sealant surfaces due to the transport of volatile Cr-containing species, such as CrO_3 or $CrO_2(OH)_2$. The high CTE of $BaCrO_4$ ($\sim 18 \times 10^{-6}$ K^{-1}), contributes to the physical separation of the sealing glass from the stack components where the CTEs are (10–13) $\times$ 10^{-6} K^{-1} [9]. Thus, the formation of low expansivity $BaAl_2Si_2O_8$ phase due to high BaO content in these glasses makes them unsuitable for the SOFC sealants.

4.3. Clinopyroxene based sealants

The pyroxenes are a wide spread group rock-forming silicate minerals found in many igneous and metamorphic rocks. The general chemical formula for pyroxenes is $M2M1T_2O_6$, where M2 refers to cations in a generally distorted octahedral coordination (Mg^{2+}, Fe^{2+}, Mn^{2+}, Li^{+}, Ca^{2+}, Na^{+}), M1 to cations in a regular octahedral coordination (Al^{3+}, Fe^{3+}, Ti^{4+}, Cr^{3+}, V^{3+}, Ti^{3+}, Zr^{4+}, Sc^{3+}, Zn^{2+}, Mg^{2+}, Fe^{2+}, Mn^{2+}), and T to tetrahedrally coordinated cations (Si^{4+}, Al^{3+}, Fe^{3+}). Any pyroxene belonging to monoclinic crystal systems are called clinopyroxene. The most significant advantage of the clinopyroxene silicate glass system is the chain silicate structure which offers incorporation of various cations [123]. The stability of clinopyroxenes over a broad spectrum of chemical compositions, in conjunction with the possibility of achieving desired physical properties and high chemical durability, has generated a great interest for their application in fuel cells as a sealant material.

Diopside (Di: $CaMgSi_2O_6$) and Ca-Tschermak (CaTs: $CaAl_2SiO_6$) are the members of the clinopyroxene group, forming a limited solid solution with the general formula $Ca(Mg_{1-x}Al_x)(Si_{1-x}Al_{x/2})_2O_6$. It is worthy to mention that, in our initial screening studies, we have been trying to determinethe solubility limit of CaTs in the structure of Di by varying the CaTs concentration from 0 to 35 mol%. It was found that up to 30 mol% CaTs are soluble in Di [20,28,124]. More interestingly, the thermal stability and crystallization kinetics studies for glasses, and the investigations of crystalline phase

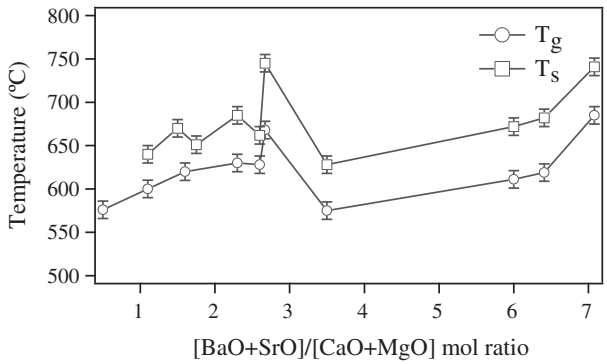

Fig. 11. Variations of glass transition (T_g) and glass softening point (T_s) vs (BaO + SrO)/(CaO + MgO) molar ratio in selected alkaline-earth aluminosilicate glass compositions (based on the data from Tables 2, 3 and 5).

evolution, density, shrinkage, mechanical strength and CTE for the corresponding GCs revealed that the properties achieved for the 80 mol% Di: 20 mol% CaTs glass composition ($CaMg_{0.8}Al_{0.4}Si_{1.8}O_6$) [124] are near the required sealant properties range [9]. However, some other parameters need to be improved, including the achievement of suitable CTE, low electrical conductivity, and low chemical interaction with the SOFC components under both air and H_2 atmosphere. In view of these challenges we have considered diopside and $CaMg_{0.8}Al_{0.4}Si_{1.8}O_6$ (80Di/20Ca–Ts) glass compositions as the parent glasses. Various clinopyroxene based glasses tested as SOFC sealants are listed in Table 5; their properties are summarized in Table 6 and Figs. 12–14 [20,28–30,32–34,39,40,124–128].

4.3.1. Influence of BaO

It was known that the addition of BaO increases the CTE of the glasses and resultant GCs [84,85,95,107,108,117–119]. Thus, partial

Table 5
Some clinopyroxene based glass compositions (%) investigated for SOFC sealants.

	CaO/MgO	BaO/SrO	Al_2O_3/La_2O_3	SiO_2	B_2O_3	Others	Ref.
Diopside-Ca-Tschermak (CaTs)							
mol	26.32/21.05	–	5.26	47.37	–	–	[28]
	21.13/22.53	–	5.63	43.66	3.52	3.52 Y_2O_3	
	21.05/21.05	5.26	2.63	47.37	2.63	–	
wt	25.86/14.87	–	9.40	49.87	–	–	
	18.70/14.35	–	9.07	41.44	3.87	12.55 Y_2O_3	
	19.24/13.83	13.15	4.37	46.40	2.98	–	
mol	26.32–27.40/17.81–21.05	–	5.26–9.59	45.20–47.37	–	–	[124]
wt	25.86–27.40/12.07–14.87	–	9.40–16.44	45.66–49.87			
mol	21.05–25/21.05	1.32–5.26	2.63–5.26	47.37	0–2.63	–	[127]
wt	19.24–24.03/13.83–14.54	3.46–13.15	4.37–9.20	46.40–48.78	0–2.98	–	
BaO and ZnO containing Di-CaTs							
mol	21.05–25/21.05	1.32–5.26/–	2.63–5.26	47.37	0–2.63	–	[125]
wt	18.9824.03/13.64–14.54	3.46–13.15/–	4.37–9.20	45.76–48.78	0–2.98	–	
mol	26.32–27.40/17.81–21.05	–	5.26–9.59	45.20–47.37	–	–	[20]
wt	25.83–25.86/14.87–12.07	–	9.40–16.44	45.66–49.87	–	–	
mol	26.32–26.3/14.87–15.8	–	5.26–5.3	47.37–47.4	–	0–5.3 ZnO 1 NiO	[126]
wt	24.91–25.86/14.87–10.74	–	9.06–9.40	48.05–49.87	–	0–7.23 ZnO 1 NiO	
mol	17.4–22.5/24.9–25	0–5	1.2/1.2–1.3	47.3–47.5	1.7–1.8	0– 0.2Cr_2O_3/0.8 NiO	[30]
wt	21.63–15.41/17.27–15.83	0–12.04	2.18–2/6.98–6.40	48.93–44.82	2	0–0.5Cr_2O_3/1 NiO	
BaO, SrO, Cr_2O_3 and R_2O_3 (R = B, Cr, Bi, La) containing compositions							
mol	20.4–20.8/23.4–25.4	2.5–2.6	1.3–2.6/1.3–2.6	46.9–48.3	–	0–0.2 Cr_2O_3/0.8–0.9 NiO	[34,40]
wt	17.86–18.82/14.44–16.90	6.11–6.43	2.14–4.06/6.83–12.97	43.06–47.88	–	0–0.5 Cr_2O_3/1 NiO	
mol	17.6–20/22–25	2.2–2.5	1.1–1.2/1.1–1.3	41.8–47.5	1.7–13.3	0.8 NiO	[34]
wt	15.97–18.44/14.34–16.56	5.46–6.30	1.81–2.09/5.80–6.70	40.62–46.91	2–15	1 NiO	
mol	17.33–17.48/22.28–22.47	–/7.43–7.49	1.24–1.25/1.24–1.25	47.04–47.44	1.79–1.87	0.83–0.87 NiO 0–0.7 Bi_2O_3	[128]
wt	14.91–15.72/13.78–14.53	–/11.81–12.45	1.94–2.04/6.19–6.53	43.37–45.72	2	1 NiO 1–5 Bi_2O_3	
mol	16.67–20.35–/20.84–25.43 19.47–20/24.33–25	2.08–2.54 –/2.43–2.50	1.04–1.27/ 1.04–1.27 1.22–1.25 1.22–1.25	39.60–48.32 46.24–47.5	0–17.89 1.71–4.30	0.81–0.83 NiO 0.80 NiO	[29]
wt	15.01–18.82/13.49 –16.90 18.25–18.83/16.40–16.92	5.13–6.43 –/4.22–4.35	1.71–2.14/ 5.45–6.83 2.07–2.14/6.63–6.84	38.20–47.88 46.44–47.92	0–20 2–5	1 NiO 1 NiO	
Diopside-Mg orthosilicate and diopside-Ba disilicate glasses							
mol	19.42–19.96/ 30.10–31.06 21.01–22.14/23.34–24.60	– 2.15–0.52	1.08–1.11/ 1.08–1.11 1.17–1.23/1.17–1.23	45.74–46.09 47.79–48.62	1.63 1.69–1.74	– 0.79–0.81 NiO	[33]
wt	19.67–19.23 21.32–22.10 19.47–21.09 15.55–16.84	1.36–5.44	1.94–1.99/6.21–6.35 1.97–2.13/6.28–6.81	48.52–48.67 48.29–48.77	2 2	– La_2O_3 1 NiO	

substitution of BaO for CaO in the glass compositions $CaMg_{0.8}Al_{0.4}Si_{1.8}O_6$ (Di-CaTs glass) and $CaMgSi_2O_6$ was carried out [28,29,34,39,40,127]. However, the content of BaO was limited in the clinopyroxene silicate glasses only up to 5.26 mol% in order to avoid the formation of low CTE celsian and high CTE $BaCrO_4$ phases. The addition of BaO in Di-CaTs glass increases the T_s from 654 to 681 °C while CTE increased from 8.0 to 8.1 $\times$ 10^{-6} K^{-1} respectively. Further, due to lower ionic field strength of BaO the crystallization activation energy E_c decreases from 437 to 378 kJ mol^{-1} with increasing BaO content in the glasses [127].

The addition of BaO to the diopside $Ca_{0.9}MgAl_{0.1}La_{0.1}Si_{1.9}O_6$ based glass increased CTE from 8.4 to 9.0 $\times$ 10^{-1} K^{-1} [39]. This behavior in diopside glasses is observed due to lowering excess molar volume V_e in the structural skeleton and thus depolymerization of glass. It has been observed that introduction of BaO increases the glass polymerization which then decreases with further additions. The increase in connectivity implies that only a part of BaO acts as network modifier. The remaining BaO might be acting as a network former and existing as interconnected BaO_4tetrahedra in the clinopyroxene glasses, similar to the network forming action of MgO [129,130]. The T_g value of ~756 °C remains almost constant in Di glass. According to Sohn et al. [119] T_g and T_s are independent of BaO content in the glasses and are proportional to the B_2O_3/SiO_2 ratio. However, Ghosh et al. [45] observed a decrease in T_g with increasing BaO concentration. This gives a strong indication that influence of each element depends on the environment.

Additionally, it has also demonstrated that addition of BaO increases the sintering ability of clinopyroxene glass, Fig. 12 [34,39]. However, along with primary augite crystalline phase ortho and hexacelsian phases were formed after prolonged heat treatments at 850 °C and 900 °C for 300 h [30,40]. Barium addition increases the activation energy for the electrical conductivity in Di based glass from 189 to 218 kJ mol^{-1} and has an opposite effect in DiCaT glasses where the activation energy decreases from 221 down to 180 kJ mol^{-1} [125]. In all cases, the electrical conductivity values are within the limits suitable for sealants. It was observed that, there are no Cr-rich zones and no occurrence of any adverse reaction between Ba and Cr at the interface.

4.3.2. Influence of ZnO

ZnO enhances sintering and crystallization processes over MgO and CaO in GCs, thus resulting into dense sintered glass powder compacts and mechanically strong GCs. Moreover, it has been observed that ZnO acts in a manner similar to B_2O_3 with regard to the viscosity and thermal expansion. In a number of alkaline-earth aluminosilicate glasses, addition of 10 mol% ZnO decreased viscosity in the transition temperature range, lowering T_g by around

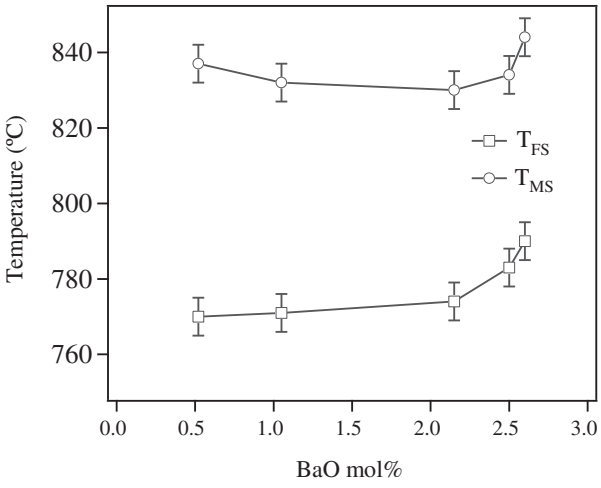

Fig. 12. First and maximum shrinkage temperatures (T_{FS} and T_{MS}) as function of BaO content in clinopyroxene based glasses [34,39].

50 °C, while at the same time slightly increasing the CTE. Also, unlike B_2O_3, ZnO remains more stable in wet hydrogen atmospheres [126,131]. In accord with the above assumptions T_g values decreased from 753 to 735 °C; CTE decreased from 8.3 to 7.6 $\times$ 10^{-6} K^{-1} with initial ZnO addition and then increased up to 7.9 $\times$ 10^{-6} K^{-1} with further doping. The behavior of T_g and CTE suggests that the addition of ZnO results in a weakening of the glass network and a decreasing of the glass viscosity. It is well recognized that ZnO [132] can act not only as network modifying oxide forming NBOs, but also enter the silicate network after 8 mol% ZnO added. Consequently, the crystallization activation energy decreases from 405 to 341 kJ mol^{-1} with increasing ZnO content up to 5.3 mol%. The activation energy for electrical conductivity increased with the initial addition of ZnO from 117 to 145 kJ mol^{-1}. Further additions of ZnO decrease it down to 50 kJ mol^{-1} and then again increase up to 87 kJ mol^{-1}.

4.3.3. Influence of La_2O_3

La_2O_3 is known to control the viscosity and CTE of the silicate glasses and GCs [119]. Therefore La_2O_3 was added to the diopside glass with the aim of altering the thermal characteristics of the glasses and the resultant GCs [40]. With increasing La_2O_3 content from 1.3 to 2.6 mol%, the T_g and T_s values decreased by 55 °C and 16 °C respectively. CTE decreased from 8.7 to 8.5 $\times$ 10^{-6} K^{-1} with increasing La_2O_3. The activation energy for crystallization has decreased from 501 to 450 kJ mol^{-1} with increasing La_2O_3 content

Table 6
Selected properties of clinopyroxene based glass and glass-ceramic compositions.

T_g, °C	T_s, °C	T_p, °C	Density (g cm^{-3}): glass/GC	Mechanical properties GC: (MPa)	CTE (10^{-6} K^{-1}): glass/GC	Act. energy for the total electrical conductivity (kJ mol^{-1})	Ref.
600–640	650–680	T_{p1}: 860–875 T_{p2}: 920–925	–/2.95–2.96	165–189	7.20–7.51 (200–500)/9.57–8.01 (200–700)		[28]
660–670	700–720	926–956	–/2.80–2.96	13.40–189.06	7.22–7.89 (200–500)		[124]
642–681	–	904–931	2.90–3.01	–	–		[127]
755–758	–	920–925	2.97–3.14/2.97–3.27	90–166	8.39–9.04(200–500)	–	[39]
927–947	–	926–956	–	–	–	–	[20]
735–753	–	904–910	2.90–3.02/2.95–3.05	–	7.61–8.31(200–600)/8.7–9.5(200–700)	87–117	[126]
–	–	–	–	–	–/8.8–9.5(200–600)	148–218	[30]
630–685	700–721	895–951	3.08–3.21/3.05–3.29	94.67–177.8	8.48–8.78(200–500)/8.29–10.3 (200–700)	–	[40]
525–550	695–710	898–905	3.11–3.22	–	8.28–8.57(200–500)/9.06–10.1(200–700)	142–157	[128]
490–685	665–716	855–912	2.98–3.08/3.01–3.15	–	7.50–8.69 (200–500)/8.62–9.69 (200–600)	147–261	[29]
–	–	873–896	–/2.96–3.19	80–189	–/9.7–11.5 (200–700)	146–178	[33]

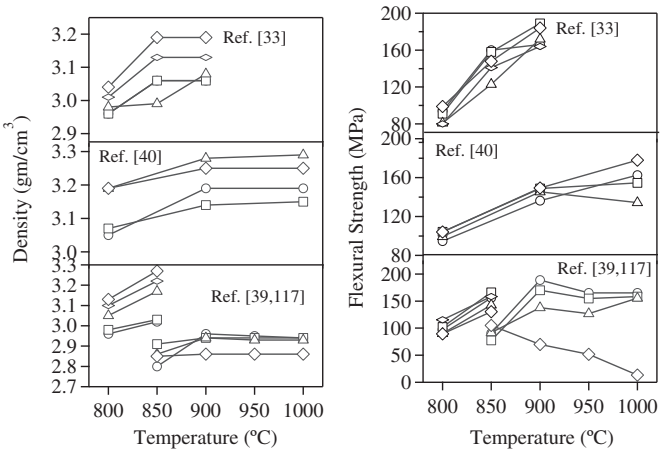

Fig. 13. Variation of density and flexural strength versus sintering temperature in different series of clinopyroxene GCs (see Table 6) [33,39,40,124].

in diopside glasses. On the other hand, there was no considerable variation in activation energy for the electrical conductivity (172 kJ mol^{-1}) of GCs in air and the obtained values obtained in the range of BaO-containing diopside glasses [125]. Overall, the addition of 1.3 mol% La_2O_3 to the diopside glasses improved the CTE of GCs.

4.3.4. Influence of B_2O_3

The decrease in viscosity and crystallization tendency of the silicate glasses (both being favorable) with the addition of B_2O_3 was also well known. According to Sohn et al. [133], B_2O_3/SiO_2 ratio plays an important role in tailoring the properties of the GC sealants as the CTE of the glasses has been observed to increase with increase in B_2O_3/SiO_2 ratio. However, considering the previously reported results and volatilization phenomena, various amounts of B_2O_3 from 5 to 20 wt.% were added to the optimized La_2O_3 and BaO-containing diopside based glass with the general formula $Ca_{0.8}Ba_{0.1}MgAl_{0.1}La_{0.1}Si_{1.9}O_6$ [29,40]. As a result, T_g and T_s values decreased from 685 to 490 °C and from 716 to 665 °C respectively with increasing B_2O_3 content. CTE of glass decreased from 8.7 to 7.5 × 10^{-6} K^{-1}. The activation energies of viscous flow for SiO_2 and B_2O_3 are 710 kJ mol^{-1} (1100–1400 °C) and 347 kJ mol^{-1}–50 kJ mol^{-1} (26–1300 °C), respectively [134]. Since, T_g of a glass is a function of its viscosity, therefore, decreasing viscosity implies a decrease in T_g. The E_c values decreased consistently with increase in B_2O_3 amount in the glasses. GCs containing 15 mol% B_2O_3 sintered at 850 °C for 1 h was highly porous and demonstrated lowest shrinkage. Improved CTE was observed only for 2 wt. % B_2O_3-containing $Ca_{0.8}Ba_{0.1}MgAl_{0.1}La_{0.1}Si_{1.9}O_6$ GCs. The activation energy for the conductivity increased with increasing B_2O_3 content up to 5 wt. % from 172 to 263 kJ mol^{-1}. Moreover, significant chemical interaction was observed, with the thickness of the Cr- and Ba-rich reaction zone at the interface between Crofer22 alloy and glass increasing with B_2O_3 content thus evidencing high reactivity. Although, the degradation of B_2O_3-containing seals under humidified reducing conditions due to the formation of volatile species has been well documented in literature [81] no such effects were observed with the very low concentration of B_2O_3 (2 wt.%) in the clinopyroxene glasses. Further, no chromate formation was identified. An addition, 2 wt.% of B_2O_3 may thus improve the clinopyroxene based sealant performance.

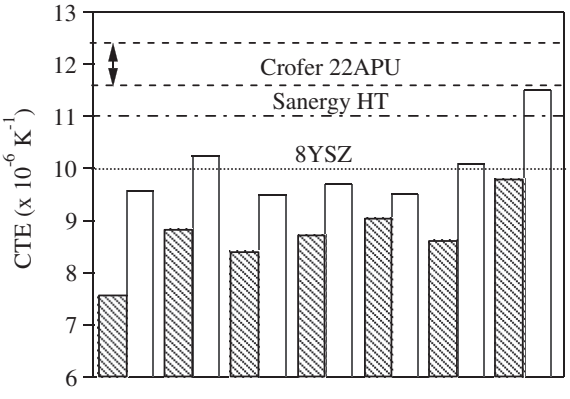

Fig. 14. Variation of CTE in different series of clinopyroxene glass (filled) and GCs (open), (compositions from diopside – CaTs series [28,124,127]; compositions from diopside – CaTs series with BaO and ZnO addition [30,126], compositions from Diopside based glasses with B_2O_3, La_2O_3 and Bi_2O_3 addtions [29,40,128], compositions from Diopside with Mg orthosilicate and Ba disilicate additions [33]) see Table 6. Average thermal expansion coefficients of 8 mol% yttria-stabilized zirconia (8YSZ) and standard interconnect alloys are shown by dashed lines.

4.3.5. Influence of Mg_2SiO_4 and $BaSi_2O_5$

The optimized $Ca_{0.9}MgAl_{0.1}La_{0.1}Si_{1.9}O_6$ with GC seal demonstrated good wetting abilities and minimal chemical interaction with the other SOFC components. However, thermal stability of these GC seals during long-term operation with appropriate CTE matching and minimal reactivity with SOFC components during long run is still a matter of concern. In order to improve the glass-ceramic compositions with combination of diopside with the crystalline phases exhibiting substantially high CTE, magnesium orthosilicate (Mg_2SiO_4: 10–12 wt.%)/barium aluminosilicates ($BaSi_2O_5$: 2.5 to 10 wt.%) [10] were added [33]. No significant variation in T_s (675 °C) was observed with the addition of Mg_2SiO_4 and $BaSi_2O_5$ in $Ca_{0.9}MgAl_{0.1}La_{0.1}Si_{1.9}O_6$ glass. However, CTE of glass increased with increasing Mg_2SiO_4 as well $BaSi_2O_5$ from 9.4 to 9.8 × 10^{-6} K^{-1} and from 7.1 to 9.5 × 10^{-6} K^{-1} respectively. From the HSM measurements it was also observed that with increasing Mg_2SiO_4 and $BaSi_2O_5$ sintering ability increased considerably. The CTE of GCs sintered at 900 °C for 1 h varied in the range (9.7–11.2) × 10^{-6} K^{-1} while after long heat treatment at 900 °C for 300 h it changed in the interval (9.7–11.5) × 10^{-6} K^{-1}. The activation energy for all the conductivity increased with increasing Mg_2SiO_4 and $BaSi_2O_5$ content in $Ca_{0.9}MgAl_{0.1}La_{0.1}Si_{1.9}O_6$ glass from 146 to 162 kJ mol^{-1} and from 140 to 178 kJ mol^{-1}, respectively. Among all the compositions $Ca_{0.9}MgAl_{0.1}La_{0.1}Si_{1.9}O_6$ glass with 2.5 mol% $BaSi_2O_5$ showed a homogeneous microstructure over the entire cross-section of the sealant/interconnect joint without gaps formation. No appreciable diffusion of elements from the investigated GCs toward the Crofer22APU and vice versa was detected. No interfacial layers, especially either Cr- or Ba-rich, that are detrimental due to their high CTE, were observed.

4.3.6. Influence of SrO

The glass with the lowest BaO content (0.52 mol%) from the previous diopside–barium disilicate series demonstrated the best adhesion to the interconnect material. However, CTE of the parent glass 7.1 × 10^{-6} K^{-1} was significantly lower than that of the GCs (~10 × 10^{-6} K^{-1}). Aiming at tailoring the CTE of parent glass and crystallized material, reducing viscosity of the glasses in the deformation temperature interval and achieving stable thermo-mechanical properties of sintered glass-powder compacts, new series of glasses was developed by partial substitution Sr for Ca in the same composition [35]. CTE of the glass increased from 7.1 to 11.3 × 10^{-6} K^{-1} with increasing SrO content in the glass. This effect can be explained due to the differences in bond lengths of Ca–O (2.38 Å) and Sr–O (2.60 Å) groups. From the HSM measurements it was observed that with increasing SrO content sintering ability

increased considerably from 7 to 35 and viscosity at 900 °C reduced from 6.5 to 6.2 dPas. After the prolonged heat treatment at 900 °C for 1000 h diopside evolved as the primary crystalline phase in all the GC. Stable and suitable CTE and mechanical strength values from all the GCs were achieved from the SrO contain GCs. Homogeneous microstructures over the entire cross-sections of the GC-interconnect joints (a) without gaps formation, (b) no appreciable diffusion of elements from GC toward Sanergy HT and vice versa, and (c) absence of any detrimental Cr or Ba-rich layers were observed. Furthermore increasing strontium concentration increased conductivity, whilst the activation energy decreased from 246 to 162 kJ mol^{-1}. Nonetheless, all the sealants possess excellent insulating properties; in the temperature range necessary for SOFC operation; their electrical resistivity is higher than 2 MOhm cm. The thermal shock resistance tests for GCs demonstrated that sealants are suitable for sealing of zirconia–based ceramics.

5. Conclusions

The difficulties in meeting all the requirements in a given material stimulated many research groups throughout world searching for novel glass sealants.

1. The alkali containing aluminosilicate glass sealants demonstrated the following features:
   (a) Glass transition (T_g) and glass softening point (T_s) continuously decrease with increasing $(Na_2O + K_2O)/(CaO + MgO)$ molar ratio.
   (b) CTE of glasses increased from 7.8 to 10.7 $\times 10^{-6}$ K^{-1} when $(Na_2O + K_2O)/(CaO + MgO)$ molar ratio changes in the range 0 to 0.4, and then decreased to about 8.2 $\times 10^{-6}$ K^{-1}. CTE values were stabilized with the further increase in $(Na_2O + K_2O)/(CaO + MgO)$ molar ratio (i.e. between 0.6 and 1.7).
   (c) The desired CTE range of (9–11) $\times 10^{-6}$ K^{-1} has been achieved when the glasses possess $(Na_2O + K_2O)/(CaO + MgO)$ molar ratio in the range 0.1–0.5.
2. Barium and/or strontium containing aluminosilicate glasses exhibit lowest T_g and T_s and highest CTE values as compared to other alkaline-earth containing glasses.
   (a) Variation in T_g and T_s are rather discontinuous: (i) when molar ratio $(BaO + SrO)/(CaO + MgO)$ ranges from 0.50 to 2.67, T_g and T_s vary in the intervals of 575–650 °C and 640–750 °C, respectively; (ii) both T_g and T_s show abrupt decreases at molar ratios from 2.67 to 3.5; (iii) sluggish increases in T_s and T_g were observed in the interval 3.5–6 followed by a significant increase at the molar ratios of 6.50–7.08.
   (b) Suitable CTE values, along with respectively low T_g and T_s have been achieved in barium-containing boron-aluminosilicate glasses. However, their poor thermal stability and unwanted chemical interaction with the SOFC components limits potential use of the BaO and B_2O_3-containing glasses.
3. The stability of clinopyroxenes over a broad spectrum of chemical compositions, in conjunction with the possibility of achieving desired physical properties and high chemical durability, have generated a great interest for their application as sealant materials
   (a) The properties of diopside (Di: $CaMgSi_2O_6$) and Ca-Tschermak (CaTs: $CaAl_2SiO_6$) GCs sealants were close to the target properties, except for CTE.
   (b) Additions of BaO (up to 5.26 mol%) improved sintering ability and caused a slight increase in CTE. However, one disadvantage of these compositions is the formation of ortho and hexacelsian crystalline phases after prolonged heat treatments.
   (c) ZnO (0–5.26 mol%) enhances sintering and crystallization processes, thus resulting in dense sintered compacts and mechanically strong GCs. Moreover, it has been observed that ZnO acts in a manner similar to B_2O_3 with regard to the viscosity and thermal expansion. T_g values for glasses decreased from 753 to 735 °C. Still CTE of sintered GCs was far from desirable values.
   (d) With La_2O_3 additions from 1.3 to 2.6 mol% T_g and T_s values decreased by 55 °C and 16 °C, respectively. Generally, the addition of 1.3 mol% La_2O_3 to the diopside glasses improved CTE of GCs. A better sintering ability and improved adhesion to 8YSZ and Crofer22APU were also observed.
   (e) B_2O_3 from 5 to 20 wt.% was incorporated into the optimized La_2O_3 and BaO-containing diopside based glass with general formula $Ca_{0.8}Ba_{0.1}MgAl_{0.1}La_{0.1}Si_{1.9}O_6$. T_g and T_s values decreased from 685 to 490 °C and from 716 to 665 °C, respectively, with increasing B_2O_3 content in clinopyroxene glasses. CTE of glasses decreased from 8.7 to 7.5 $\times 10^{-6}$ K^{-1}. GCs containing 15 mol% B_2O_3 sintered at 850 °C for 1 h were highly porous and demonstrated lowest shrinkage. Appropriate CTE value was observed only for 2 wt.% B_2O_3. Moreover, chemical interaction between Crofer22 alloy and glass increased with increasing B_2O_3 content.
   (f) The optimized $Ca_{0.9}MgAl_{0.1}La_{0.1}Si_{1.9}O_6$ with (2 wt.% B_2O_3 + 1 wt.% NiO) GC seal demonstrated good wetting abilities and minimal chemical interaction with other SOFC components. However, thermal stability of these GC seals during long-term operation with appropriate CTE matching and minimal reactivity with SOFC components during long run was still a matter of concern. Thus Mg_2SiO_4 and $BaSi_2O_5$ have been introduced into $Ca_{0.9}MgAl_{0.1}La_{0.1}Si_{1.9}O_6$ glass. No significant variation in T_s was observed. However, CTE of glass with Mg_2SiO_4 as well $BaSi_2O_5$ additions increased from 9.4 to 9.8 $\times 10^{-6}$ K^{-1} and from 7.1 to 9.5 $\times 10^{-6}$ K^{-1}, respectively. Regarding the chemical interactions with interconnect among all the compositions $Ca_{0.9}MgAl_{0.1}La_{0.1}Si_{1.9}O_6$ glass with 2.5 mol% $BaSi_2O_5$ showed a homogeneous microstructure over the entire cross-section of the joint without gaps formation.
   (g) The new series of glasses developed by partial substitution Sr for Ca in above mentioned glass exhibited CTE in the range 7.1–11.3 $\times 10^{-6}$ K^{-1}. Upon increasing SrO content the sintering ability was improved whilst viscosity measured at 900 °C reduced from 6.5 to 6.2 dPas. These features along with the excellent insulating properties and high thermal shock resistance suggest new glasses as appropriate sealants for SOFCs and other high-temperature electrochemical devices based on the stabilized zirconia solid electrolytes.

Acknowledgements

Important experimental contributions, partly reviewed in this work, and helpful discussions made by A. Goel, A.A. Yaremchenko, E.V. Tsipis and M.J. Pascual are gratefully acknowledged. Also authors greatefully acknowledge CICECO, University of Aveiro, Portugal, for the experimental facilities. This work was partially supported by the FCT, Portugal (projects PTDC/CTM-CER/114209/2009 and PEst-C/CTM/LA0011/2011), the Australian Research Council – Discovery Projects (No. DP110102662), and the Ministry of Education and Science of the Russian Federation (agreement No. 8649).

References

[1] Fuel Cell Handbook, sixth ed., EG&G Technical Services, Science Applications International Corporation, Morgantown, West Virginia, 2002.
[2] N.Q. Minh, T. Takahashi, Science and Technology of Ceramic Fuel Cells, Elsevier, Amsterdam, 1995.
[3] N. Sammes, Fuel Cell Technology: Reaching Towards Commercialization, Springer, London, 2006.
[4] M.V. Perfilyev, A.K. Demin, B.L. Kuzin, A.S. Lipilin, High-temperature Electrolysis of Gases, Nauka, Moscow, 1988.
[5] E.V. Tsipis, V.V. Kharton, J. Solid State Electrochem. 15 (2011) 1007–1040.
[6] P.J. Gellings, H.J.M. Bouwmeester (Eds.), Handbook of Solid State Electrochemistry, CRC Press, Boca Raton, 1997.
[7] V.V. Kharton (Ed.), Solid State Electrochemistry I: Fundamentals, Materials and Their Applications, Wiley-VCH, Weinheim, 2009.
[8] S. Zhuiykov, Electrochemistry of Zirconia Gas Sensors, CRC Press, Boca Raton, 2007.
[9] J.W. Fergus, J. Power Sources 147 (2005) 46–57.
[10] M.K. Mahapatra, K. Lu, Mater. Sci. Eng. R 67 (2010) 65–85.
[11] M.K. Mahapatra, K. Lu, J. Power Sources 195 (2010) 7129–7139.
[12] P.A. Lessing, J. Mater. Sci. 42 (2007) 3465–3476.
[13] V. Lawlor, S. Griesser, G. Buchinger, A.G. Olabi, S. Cordiner, D. Meissner, J. Power Sources 193 (2009) 387–399.
[14] L.A. Xue, J. Yamanis, J. Piascik, E.T. Ong, US patent 7521387, 2009.
[15] S.G. Warrier, J. Yamanis, S. Tulyani, R.C. Benn, US patent 7977004, 2011.
[16] Y.S. Yoo, Y.H. Han, T.K. Kang, US patent 6864009, 2005.
[17] E.M. Badding, E.J. Cortright, T.D. Ketcham, M.D. Lineman, J.D. Julien, Y. Sun, Eur. patent 1446847, 2002.
[18] R. Draper, G. Zhang, R.J. Ruka, K.P. Litzinger, P.R. Zafred, R.A. Basel, US patent 8097381, 2012.
[19] H.J. Ko, H.W. Lee, J.C. Lee, J.H. Lee, H.S. Song, J.S. Kim, T.W. Noh, US patent 0147866 A1, 2005.
[20] A. Goel, E.R. Shaaban, D.U. Tulyaganov, J.M.F. Ferreira, J. Am. Ceram. Soc. 91 (2008) 2690–2697.
[21] J. Tong, M. Han, S.C. Singhal, Y. Gong, J. Non-Cryst. Solids 358 (2012) 1038–1043.
[22] F. Smeacetto, A. Chrysanthou, M. Salvo, T. Moskalewicz, F. D'Herin Bytner, L.C. Ajitdoss, M. Ferraris, Int. J. Hydrogen Energy 36 (2011) 11,895–11,903.
[23] H.-T. Chang, C.-K. Lin, C.-K. Liu, S.-H. Wu, J. Power Sources 196 (2011) 3583–3591.
[24] J. Schneider, V.R. Mastelaro, H. Panepucci, E.D. Zanotto, J. Non-Cryst. Solids 273 (2000) 8–18.
[25] M. Dominique, F. Franck, C. Mickael, K. Ian, C. Stphanie Le, A. Bruno, D. Jean-Olivier, B. Bruno, G. Zhehong, H. Gina, Magn. Reson. Chem. 40 (2002) 70–76.
[26] H.R. Fernandes, D.U. Tulyaganov, A. Goel, J.M.F. Ferreira, J. Eur. Ceram. Soc. 32 (2012) 291–298.
[27] A.A. Reddy, A. Goel, D.U. Tulyaganov, S. Kapoor, K. Pradeesh, M.J. Pascual, J.M.F. Ferreira, J. Power Sources 231 (2013) 203–212.
[28] A. Goel, D.U. Tulyaganov, S. Agathopoulos, M.J. Ribeiro, R.N. Basu, J.M.F. Ferreira, J. Eur. Ceram. Soc. 27 (2007) 2325–2331.
[29] A. Goel, D.U. Tulyaganov, V.V. Kharton, A.A. Yaremchenko, S. Eriksson, J.M.F. Ferreira, J. Power Sources 189 (2009) 1032–1043.
[30] A. Goel, D.U. Tulyaganov, V.V. Kharton, A.A. Yaremchenko, J.M.F. Ferreira, J. Power Sources 195 (2010) 522–526.
[31] M.J. Pascual, A. Duran, L. Pascual, J. Non-Cryst. Solids 306 (2002) 58–69.
[32] A. Goel, A.A. Reddy, M.J. Pascual, L. Gremillard, A. Malchere, J.M.F. Ferreira, J. Mater. Chem. 22 (2012) 10,042–10,054.
[33] A.A. Reddy, D.U. Tulyaganov, A. Goel, M.J. Pascual, V.V. Kharton, E.V. Tsipis, J.M.F. Ferreira, Int. J. Hydrogen Energy 37 (2012) 12,528–12,539.
[34] A. Goel, D.U. Tulyaganov, M.J. Pascual, E.R. Shaaban, F. Muñoz, Z. Lü, J.M.F. Ferreira, J. Non-Cryst. Solids 356 (2010) 1070–1080.
[35] A.A. Reddy, D.U. Tulyaganov, M.J. Pascual, V.V. Kharton, E.V. Tsipis, V.A. Kolotygin, J.M.F. Ferreira, Int. J. Hydrogen Energy 38 (2013) 3073–3086.
[36] A.A. Reddy, D.U. Tulyaganov, S. Kapoor, A. Goel, M.J. Pascual, V.V. Kharton, J.M.F. Ferreira, RSC Adv. 2 (2012) 10,955–10,967.
[37] W. Liu, X. Sun, M. Khaleel, J. Power Sources 185 (2008) 1193–1200.
[38] W.N. Liu, X. Sun, B. Koeppel, M. Khaleel, Int. J. Appl. Ceram. Technol. 7 (2010) 22–29.
[39] A. Goel, D.U. Tulyaganov, A.M. Ferrari, E.R. Shaaban, A. Prange, F. Bondioli, J.M.F. Ferreira, J. Am. Ceram. Soc. 93 (2010) 830–837.
[40] A. Goel, D.U. Tulyaganov, V.V. Kharton, A.A. Yaremchenko, J.M.F. Ferreira, Acta Mater. 56 (2008) 3065–3076.
[41] P.H. Larsen, F.W. Poulsen, R.W. Berg, J. Non-Cryst. Solids 244 (1999) 16–24.
[42] S. Ghosh, A. Das Sharma, P. Kundu, S. Mahanty, R.N. Basu, J. Non-Cryst. Solids 354 (2008) 4081–4088.
[43] N.P. Bansal, E.A. Gamble, J. Power Sources 147 (2005) 107–115.
[44] K.D. Meinhardt, D.S. Kim, Y.S. Chou, K.S. Weil, J. Power Sources 182 (2008) 188–196.
[45] S. Ghosh, P. Kundu, A. Das Sharma, R.N. Basu, H.S. Maiti, J. Eur. Ceram. Soc. 28 (2008) 69–76.
[46] Z. Yang, Solid State Ionics 160 (2003) 213–225.
[47] E.V. Stephens, J.S. Vetrano, B.J. Koeppel, Y. Chou, X. Sun, M.A. Khaleel, J. Power Sources 193 (2009) 625–631.
[48] K.D. Meinhardt, J.D. Vienna, T.R. Armstrong, L.R. Pederson, US patent 6430966 B1, 2002.
[49] P.H. Larsen, P.F. James, J. Mater. Sci. 33 (1998) 2499–2507.
[50] W.N. Liu, X. Sun, M.A. Khaleel, J. Power Sources 196 (2011) 1750–1761.
[51] S.M. Gross, D. Federmann, J. Remmel, M. Pap, J. Power Sources 196 (2011) 7338–7342.
[52] M.J. Pascual, A. Guillet, A. Durán, J. Power Sources 169 (2007) 40–46.
[53] I.W. Donald, P.M. Mallinson, B.L. Metcalfe, L.A. Gerrard, J.A. Fernie, J. Mater. Sci. 46 (2011) 1975–2000.
[54] I.W. Donald, B.L. Metcalfe, L.A. Gerrard, J. Am. Ceram. Soc. 91 (2008) 715–720.
[55] D. Coillot, F.O. Méar, R. Podor, L. Montagne, Adv. Funct. Mater. 20 (2010) 4371–4374.
[56] N. Govindaraju, W.N. Liu, X. Sun, P. Singh, R.N. Singh, J. Power Sources 190 (2009) 476–484.
[57] R.N. Singh, Int. J. Appl. Ceram. Technol. 4 (2007) 134–144.
[58] T. Zhang, D. Tang, H. Yang, J. Power Sources 196 (2011) 1321–1323.
[59] Z. Teng, Z. Qi, Z. Jing, T. Dian, Y. Hiswen, J. Power Sources 204 (2012) 122–126.
[60] R.N. Singh, J. Mater. Res. 27 (2012) 2055–2061.
[61] R.N. Singh, S.S. Parihar, Self healing behavior of glasses for high temperature seals in solid oxide fuel cells, in: N.P. Bansal, J. Salem, D. Zhu (Eds.), Advances in Solid Oxide Fuel Cells III: Ceramic and Engineering Science Proceeding, vol. 28, John Wiley & Sons, Hoboken, NJ, USA, 2009. Issue 4.
[62] R.N. Singh, S.S. Parihar, Performance of self-healing seals for solid oxide fuel cells (SOFC), in: N.P. Bansal, A. Wereszczak, E. Lara-Curzio (Eds.), Advances in Solid Oxide Fuel Cells II: Ceramic Engineering and Science Proceedings, vol. 27, John Wiley & Sons, Hoboken, NJ, USA, 2008. Issue 4.
[63] G.V. Kukolev, Silicon Chemistry and Physical Chemistry of Silicates, Higher School Publ., Moscow, 1966.
[64] H.R. Fernandes, D.U. Tulyaganov, A. Goel, M.J. Ribeiro, M.J. Pascual, J.M.F. Ferreira, J. Eur. Ceram. Soc. 30 (2010) 2017–2030.
[65] J.E. Shelby, Introduction to Glass Science and Technology, The Royal Society of Chemistry, Cambridge, 1997.
[66] P. Ganster, M. Benoit, W. Kob, J.M. Delaye, J. Chem. Phys. 120 (2004) 10,172–10,181.
[67] K. Bhupinder, K. Singh, O.P. Pandey, Int. J. Hydrogen Energy 37 (2012) 3839–3847.
[68] Y.-S. Chou, E.C. Thomsen, J.P. Choi, J.W. Stevenson, J. Power Sources 197 (2012) 154–160.
[69] Y.-S. Chou, E.C. Thomsen, R.T. Williams, J.P. Choi, N.L. Canfield, J.F. Bonnett, J.W. Stevenson, A. Shyam, E. Lara-Curzio, J. Power Sources 196 (2011) 2709–2716.
[70] D. Coillot, F.O. Méar, H. Nonnet, L. Montagne, Int. J. Hydrogen Energy 37 (2012) 9351–9358.
[71] F. Smeacetto, M. Salvo, F.D. D'Hérin Bytner, P. Leone, M. Ferraris, J. Eur. Ceram. Soc. 30 (2010) 933–940.
[72] F. Smeacetto, M. Salvo, M. Ferraris, V. Casalegno, P. Asinari, J. Eur. Ceram. Soc. 28 (2008) 611–616.
[73] F. Smeacetto, M. Salvo, M. Ferraris, J. Cho, A.R. Boccaccini, J. Eur. Ceram. Soc. 28 (2008) 61–68.
[74] F. Smeacetto, A. Chrysanthou, M. Salvo, Z. Zhang, M. Ferraris, J. Power Sources 190 (2009) 402–407.
[75] F. Smeacetto, M. Salvo, M. Ferraris, V. Casalegno, P. Asinari, A. Chrysanthou, J. Eur. Ceram. Soc. 28 (2008) 2521–2527.
[76] S. Lee, B. Mysen, G. Cody, Phys. Rev. B 68 (2003) 214,206.
[77] S.K. Lee, J.F. Stebbins, J. Phys. Chem. B 107 (2003) 3141–3148.
[78] V.V. Kharton, E.N. Naumovich, A.A. Vecher, J. Solid State Electrochem. 3 (1999) 61–81.
[79] T. Zhang, R.K. Brow, W.G. Fahrenholtz, S.T. Reis, J. Power Sources 205 (2012) 301–306.
[80] T. Zhang, H. Zhang, G. Li, H. Yung, J. Power Sources 195 (2010) 6795–6797.
[81] T. Zhang, W.G. Fahrenholtz, S.T. Reis, R.K. Brow, J. Am. Ceram. Soc. 91 (2008) 2564–2569.
[82] F. Heydari, A. Maghsoudipour, Z. Hamnabard, S. Farhangdoust, Mater. Sci. Eng. A 552 (2012) 119–124.
[83] S.R. Choi, N.P. Bansal, A. Garg, Mater. Sci. Eng. A 460, 461 (2007) 509–515.
[84] A. Arora, K. Singh, O.P. Pandey, Int. J. Hydrogen Energy 36 (2011) 14,948–14,955.
[85] A. Arora, V. Kumar, K. Singh, O.P. Pandey, Ceram. Int. 37 (2011) 2101–2107.
[86] Y.S. Chou, J.W. Stevenson, G.G. Xia, Z.G. Yang, J. Power Sources 195 (2010) 5666–5673.
[87] Y.-S. Chou, J.W. Stevenson, K.D. Meinhardt, J. Am. Ceram. Soc. 93 (2010) 618–623.
[88] Y.-S. Chou, J.W. Stevenson, P. Singh, J. Power Sources 184 (2008) 238–244.
[89] S.-F. Wang, Y.-F. Hsu, H.-C. Lu, S.-C. Lo, C.-S. Cheng, Int. J. Hydrogen Energy 37 (2012) 5901–5913.
[90] K. Sharma, G.P. Kothiyal, L. Montagne, F.O. Méar, B. Revel, Int. J. Hydrogen Energy 37 (2012) 11,360–11,369.
[91] B. Tiwari, A. Dixit, G.P. Kothiyal, Int. J. Hydrogen Energy 36 (2011) 15,002–15,008.
[92] A. Ananthanarayanan, G.P. Kothiyal, L. Montagne, G. Tricot, B. Revel, Mater. Chem. Phys. 130 (2011) 880–889.
[93] G. Kaur, O.P. Pandey, K. Singh, Int. J. Hydrogen Energy 37 (2012) 6862–6874.
[94] V. Kumar, S. Sharma, O.P. Pandey, K. Singh, Solid State Ionics 181 (2010) 79–85.

[95] V. Kumar, O.P. Pandey, K. Singh, Ceram. Int. 36 (2010) 1621–1628.
[96] V. Kumar, A. Arora, O. Pandey, K. Singh, Int. J. Hydrogen Energy 33 (2008) 434–438.
[97] P.K. Ojha, S.K. Rath, T.K. Chongdar, N.M. Gokhale, A.R. Kulkarni, J. Power Sources 196 (2011) 4594–4598.
[98] T. Jin, K. Lu, J. Power Sources 195 (2010) 195–203.
[99] M.K. Mahapatra, K. Lu, J. Mater. Sci. 44 (2009) 5569–5578.
[100] K. Lu, M.K. Mahapatra, J. Appl. Phys. 104 (2008) 074910.
[101] C.-K. Lin, J.-Y. Chen, J.-W. Tian, L.-K. Chiang, S.-H. Wu, J. Power Sources 205 (2012) 307–317.
[102] H.-T. Chang, C.-K. Lin, C.-K. Liu, J. Power Sources 195 (2010) 3159–3165.
[103] H.-T. Chang, C.-K. Lin, C.-K. Liu, J. Power Sources 189 (2009) 1093–1099.
[104] J. Hao, Q. Zan, D. Ai, J. Ma, C. Deng, J. Xu, J. Power Sources 214 (2012) 75–83.
[105] D. Gödeke, U. Dahlmann, J. Power Sources 196 (2011) 9046–9050.
[106] S.-F. Wang, C.-M. Lu, Y.-C. Wu, Y.-C. Yang, T.-W. Chiu, Int. J. Hydrogen Energy 36 (2011) 3666–3672.
[107] T. Sun, H. Xiao, W. Guo, X. Hong, Ceram. Int. 36 (2010) 821–826.
[108] S.-F. Wang, Y.-R. Wang, Y.-F. Hsu, C.-C. Chuang, Int. J. Hydrogen Energy 34 (2009) 8235–8244.
[109] S.J. Widgeon, E.L. Corral, M.N. Spilde, R.E. Loehman, J. Am. Ceram. Soc. 92 (2009) 781–786.
[110] N. Laorodphan, P. Namwong, W. Thiemsorn, M. Jaimasith, A. Wannagon, T. Chairuangsri, J. Non-Cryst. Solids 355 (2009) 38–44.
[111] Y. Zhao, J. Malzbender, S.M. Gross, J. Eur. Ceram. Soc. 31 (2011) 541–548.
[112] M.K. Mahapatra, K. Lu, R.J. Bodnar, Appl. Phys. A 95 (2008) 493–500.
[113] C.Y.S. Chang, W.C.J. Wei, C.H. Hsueh, J. Non-Cryst. Solids 357 (2011) 1414–1419.
[114] V. Kumar, O. Rupali, P. Pandey, K. Singh, Int. J. Hydrogen Energy 36 (2011) 14,971–14,976.
[115] P.K. Ojha, T.K. Chongdar, N.M. Gokhale, A.R. Kulkarni, Int. J. Hydrogen Energy 36 (2011) 14,996–15,001.
[116] M.K. Mahapatra, K. Lu, X. Liu, J. Wu, Int. J. Hydrogen Energy 35 (2010) 7945–7956.
[117] L. Peng, Q. Zhu, J. Power Sources 194 (2009) 880–885.
[118] Y.-S. Chou, J.W. Stevenson, P. Singh, J. Electrochem. Soc. 154 (2007) B644.
[119] S.-B. Sohn, S.-Y. Choi, G.-H. Kim, H.-S. Song, G.-D. Kim, J. Non-Cryst. Solids 297 (2002) 103–112.
[120] T. Zhang, Q. Zou, F. Zeng, S. Wang, D. Tang, H. Yang, J. Power Sources 216 (2012) 1–4.
[121] M.B. Volf, Glass Science and Technology, Elsevier, Amsterdam, 1984.
[122] N. Lahl, K. Singh, L. Singheiser, K. Hilpert, D. Bahadur, J. Mater. Sci. 35 (2000) 3089–3096.
[123] N. Morimoto, J. Fabries, A.K. Ferguson, I.V. Ginzburg, M. Ross, F.A. Seifert, J. Zussman, K. Aoki, G. Gottardi, Am. Mineralogist 73 (1988) 1123–1133.
[124] A. Goel, D.U. Tulyaganov, S. Agathopoulos, M.J. Ribeiro, J.M.F. Ferreira, J. Eur, Ceram. Soc. 27 (2007) 3231–3238.
[125] A. Goel, D.U. Tulyaganov, V.V. Kharton, A.A. Yaremchenko, S. Agathopoulos, J.M.F. Ferreira, J. Am. Ceram. Soc. 90 (2007) 2236–2244.
[126] A. Goel, D.U. Tulyaganov, E.R. Shaaban, R.N. Basu, J.M.F. Ferreira, J. Appl. Phys. 104 (2008) 043529.
[127] A. Goel, D.U. Tulyaganov, I.K. Goel, E.R. Shaaban, J.M.F. Ferreira, J. Non-Cryst. Solids 355 (2009) 193–202.
[128] A. Goel, M.J. Pascual, J.M.F. Ferreira, Int. J. Hydrogen Energy 35 (2010) 6911–6923.
[129] R.K. Mishra, V. Sudarsan, C.P. Kaushik, K. Raj, S.K. Kulshreshtha, A.K. Tyagi, J. Non-Cryst. Solids 353 (2007) 1612–1617.
[130] K.S. Kim, P.J. Bray, Phys. Chem. Glasses 15 (1974) 47–51.
[131] Gmelin's Handbook of Inorganic Chemistry, Chemie, Leipzig, 1992.
[132] L. Linati, G. Lusvardi, G. Malavasi, L. Menabue, M.C. Menziani, P. Mustarelli, U. Segre, J. Phys. Chem. B 109 (2005) 4989–4998.
[133] S.-B. Sohn, S.-Y. Choi, J. Am. Ceram. Soc. 87 (2004) 254–260.
[134] R.H. Doremus, in: Glass Science, second ed., John Wiley & Sons, Inc., USA, 1994.